

April 2014

# Partially Enclosed Vertical Axis Wind Turbine

Jefferson C. Lee

*Worcester Polytechnic Institute*

Mark Haywood Shooter

*Worcester Polytechnic Institute*

Paige T. Archinal

*Worcester Polytechnic Institute*

Ryan J. Pollin

*Worcester Polytechnic Institute*

Follow this and additional works at: <https://digitalcommons.wpi.edu/mqp-all>

---

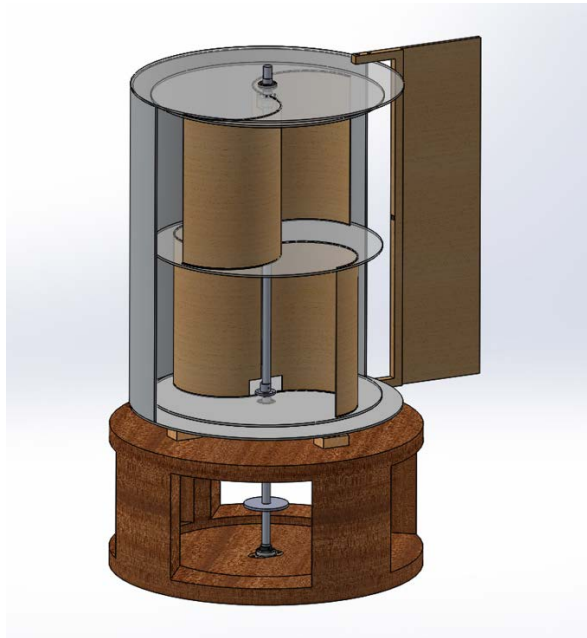
## Repository Citation

Lee, J. C., Shooter, M. H., Archinal, P. T., & Pollin, R. J. (2014). *Partially Enclosed Vertical Axis Wind Turbine*. Retrieved from <https://digitalcommons.wpi.edu/mqp-all/1894>

This Unrestricted is brought to you for free and open access by the Major Qualifying Projects at Digital WPI. It has been accepted for inclusion in Major Qualifying Projects (All Years) by an authorized administrator of Digital WPI. For more information, please contact [digitalwpi@wpi.edu](mailto:digitalwpi@wpi.edu).

WORCESTER POLYTECHNIC INSTITUTE  
PROJECT ID: BJS – WS14

# Partially Enclosed Vertical Axis Wind Turbine



Major Qualifying Project 2013-2014

**Paige Archinal, Jefferson Lee, Ryan Pollin, Mark Shooter**

**4/24/2014**

## Acknowledgments

We would like to thank Professor Brian Savilonis for his guidance throughout this project. We would like to thank Herr Peter Hefti for providing and maintaining an excellent working environment and ensuring that we had everything we needed. We would especially like to thank Kevin Arruda and Matt Dipinto for their manufacturing expertise, without which we would certainly not have succeeded in producing a product.

## Abstract

Vertical Axis Wind Turbines (VAWTs) are a renewable energy technology suitable for low-speed and multidirectional wind environments. Their smaller scale and low cut-in speed make this technology well-adapted for distributed energy generation, but performance may still be improved. The addition of a partial enclosure across half the front-facing swept area has been suggested to improve the coefficient of performance, but it undermines the multidirectional functionality. To quantify its potential gains and examine ways to mitigate the losses of unidirectional functionality, a Savonius blade VAWT with an independently rotating enclosure with a passive tail vane control was designed, assembled, and experimentally tested. After analyzing the output of the system under various conditions, it was concluded that this particular enclosure shape drastically reduces the coefficient of performance of a VAWT with Savonius blades. However, the passive tail vane rotated the enclosure to the correct orientation from any offset position, enabling the potential benefits of an advantageous enclosure design in multidirectional wind environments.

# Executive Summary

## Introduction

Vertical Axis Wind Turbines (VAWTs) are a renewable energy technology suitable for low-speed and multidirectional wind environments. Their smaller scale and low cut-in speed make this technology well-adapted for distributed energy distribution, but performance may still be improved. The addition of a partial enclosure across half the front-facing swept area has been suggested to improve the coefficient of performance, but it undermines the multidirectional functionality.

A partial enclosure surrounding could reduce the wind striking the returning blades and increase the flow speed flowing into the advancing blade (Mohamed, 2010). Previous research by Brandmaier, et al. specifies an enclosure shape for a flat-plate bladed VAWT, optimized with flow simulation and verified experimentally at a small scale (Brandmaier, et al. 2012). To ensure that the benefits of the enclosure will be realized, it must be in the optimal position, which changes with varying wind direction. The simplest passive system utilizes a tail vane to align the turbine into the wind.

Based on the research outlined above, a two-stage, Savonius-bladed VAWT with a passive tail vane was constructed. The optimized enclosure shape from Brandmaier, et al. was scaled up to fit the new turbine.

There were two objectives to the project, which build the body of research on enclosures relating to VAWTs. First, the project quantified the effects of an enclosure on the coefficient of performance of a near-market scale Savonius-bladed VAWT. Second, the project designed and evaluated a wind direction control system to align the proposed enclosure in an environment with changing wind direction. Figure 1 below shows the VAWT fully constructed and under testing.

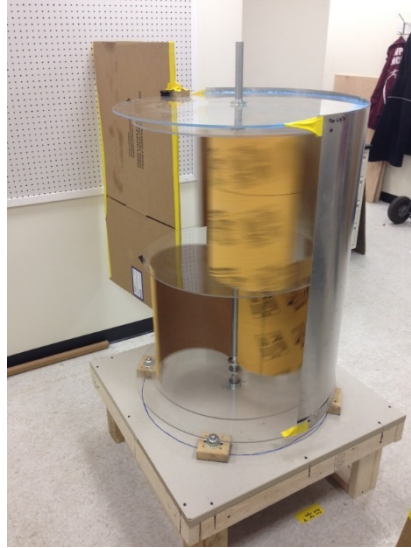


Figure 1: VAWT and Enclosure/Tail Vane System under Testing

## Methodology

After construction of the turbine, base, and enclosure, various experimental tests were designed and conducted with the purpose of quantifying the coefficient of performance, as well as torque and power output of the VAWT. A large floor fan provided constant wind speed for all experimental tests. Mechanical torque of the system was measured using a brake dynamometer. The brake dynamometer device consisted of a strap looped around a pulley on the shaft of the turbine. A load was applied with the strap to provide a torque against the rotation of the shaft. By measuring the turbine angular velocity over increasing torques applied by the brake dynamometer, a power curve can be generated, and subsequently the coefficient of performance.

To quantify the performance of the wind direction device, an experiment was performed that measured the time elapsed as the enclosure and tail vane return to the correct orientation after being initially set at an offset position. This test was conducted at  $45^\circ$ ,  $90^\circ$ ,  $135^\circ$ ,  $180^\circ$ ,  $-135^\circ$ ,  $-90^\circ$ , and  $-45^\circ$  degrees offset from the correct orientation. Figure 2 below demonstrates this experimental set up.

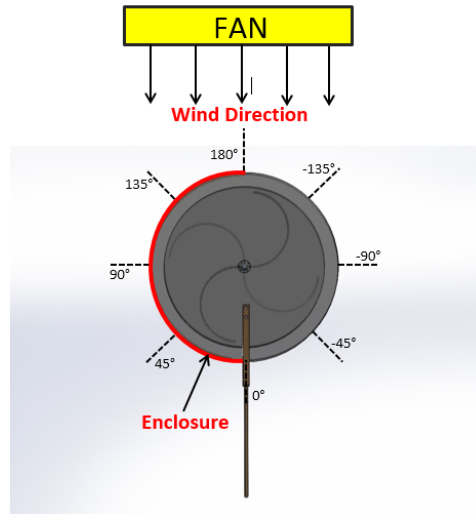


Figure 2: Tail Vane Experimental Setup

## Results

After analyzing the output of the system under various conditions, it was concluded that this particular enclosure shape drastically reduces all performance of a VAWT with Savonius blades. Figure 3 below shows the mechanical power output of the turbine with and without the enclosure for the higher of two tested wind speeds. The results are typical of both wind speeds.

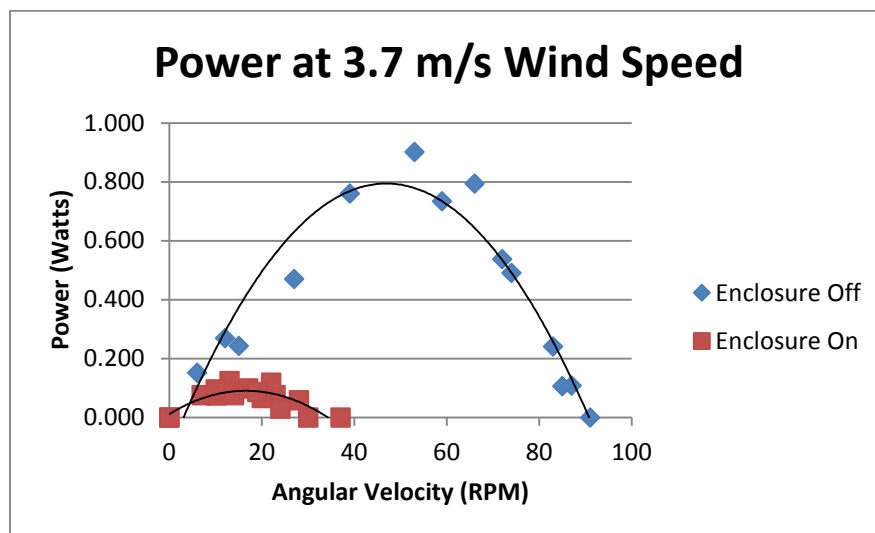


Figure 3: Effect of Enclosure on VAWT Output Power

The effects of the enclosure are summarized in Table 1, below.

Table 1: Summary of Enclosure Validation Tests

Observed Property	Percent Change
Torque, low wind	-56%
Torque, high wind	-86%
Power, low wind	-49%
Power, high wind	-92%
Coefficient of Performance, low wind	-83%
Coefficient of Performance, high wind	-72%

The wind direction control device was a passively controlled tail vane. The tail vane aligned the turbine very well at all angles, as seen below in Figure 4.

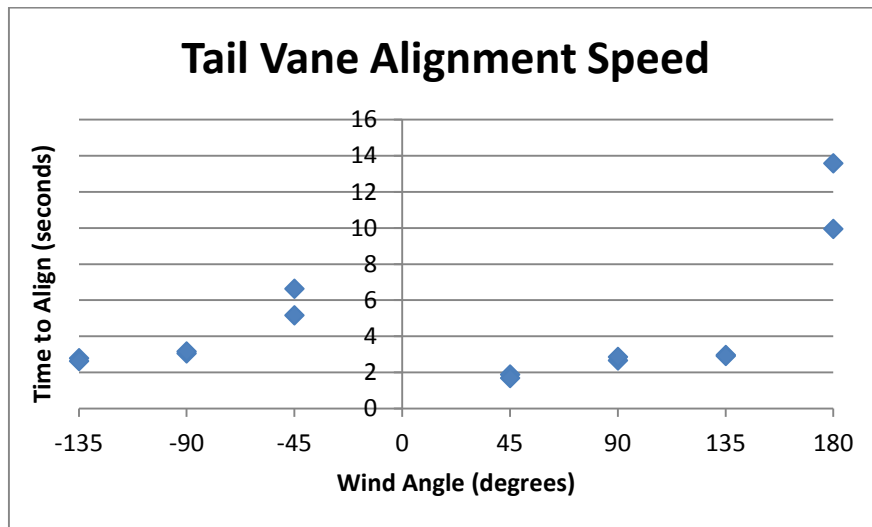


Figure 4: Tail Vane Alignment Reaction Speed

## Discussion

The performance of the VAWT with the enclosure was surprising, since the previous data for drag-based blades showed significant improvements in coefficient of performance. Two primary factors can be attributed to this difference: the blade shape and the gap between turbine and enclosure. Moving from flat blades to Savonius blades made a significant change in the solidity of the turbine,



which heavily influences the flow of air through the swept area. Second, the specifications of the enclosure by Brandmaier, et al., were interpreted in a way such that the distance between the turbine and enclosure was unspecified. This dimension likely has an impact on the performance of an enclosure, and was not investigated here.

After it was determined that the enclosure reduced the coefficient of performance, some ad hoc experimentation led to a new conceptual path for an enclosure for Savonius blades. The proposed concept focuses on a funnel or Venturi effect leading into half the swept area, and led to a power increase of 34% over the turbine with no enclosure. Future efforts to design an enclosure for Savonius bladed VAWTs could focus on an enclosure that operates principally as a funnel seem to be much more fruitful than an enclosure that blocks wind from the returning blades, the desired effect of the Brandmaier enclosure.

The performance of the tail vane exceeded expectations. Regardless of the wind direction, the tail vane reoriented the enclosure to the correct position in a matter of seconds. It should also be noted that any change in the enclosure shape likely warrants a full redesign of the wind direction control device as the enclosure has a significant effect on the wind profile of the VAWT assembly.

## Conclusion

The goal of the project is to design, build, and evaluate a Savonius VAWT prototype with a partial enclosure proposed by Brandmaier, et al., and a wind alignment device. Through experimental testing, the enclosure was found to reduce the torque output, power output, and the coefficient of performance of the VAWT in both low and high wind speed configurations. Results from brake dynamometer measurements of the turbine with the partial enclosure attached exhibited decreases in coefficient of performance by 83% and 72%, torque output by 56% and 86%, power output by 49% and 92%, for low and high wind speed, respectively. The tail vane however, was successful in rotating the enclosure to the correct orientation regardless of the wind direction.

# Table of Contents

Acknowledgments.....	2
Abstract.....	3
Executive Summary.....	4
Introduction .....	4
Methodology.....	5
Results.....	6
Discussion .....	7
Conclusion.....	8
List of Figures .....	11
List of Tables .....	13
Introduction .....	14
Project Goal.....	15
Literature Review .....	16
Savonius vs. Darrieus Blades.....	16
Optimal Rotor and Blade Design.....	16
Enclosure.....	23
Alignment Methods .....	24
Design Overview .....	28
Mathematical Modeling.....	28
Size and Geometry .....	32
Blades.....	33
Enclosure and Wind-Alignment Device .....	35
Materials .....	36
Assembly .....	38
Design Iterations .....	39
Turbine .....	41
Enclosure and Tail Vane .....	42
Base and Downstream Mechanical Components .....	43
Methodology.....	44
Results.....	48
Enclosure Verification .....	48
Direction Control.....	51
Discussion .....	53

Enclosure Verification .....	53
Direction Control.....	54
Recommendations .....	56
Enclosure Verification .....	56
Directional Control.....	58
Conclusion.....	59
Bibliography .....	60
Appendices.....	63
Appendix A: Design Proof Calculations.....	63
Appendix B: Material Detail Matrices.....	83
Appendix C: Prototype Fabrication.....	<b>Error! Bookmark not defined.</b>

## List of Figures

Figure 1: VAWT and Enclosure/Tail Vane System under Testing.....	5
Figure 2: Tail Vane Experimental Setup .....	6
Figure 3: Effect of Enclosure on VAWT Output Power .....	6
Figure 4: Tail Vane Alignment Reaction Speed .....	7
Figure 5: VAWT Turbines with Varying Stages (Saha et al., 2008).....	17
Figure 6: Traditional Savonius blades (Mohamed, Janiga, Pap, & Thevenin, 2010).....	19
Figure 7: Savonius Blade Optimization (Mohamed, 2011) .....	20
Figure 8: Optimum Savonius Blade Comparison (Mohamed, 2011) .....	21
Figure 9: Modified Savonius Rotor (Menet, 2001) .....	22
Figure 10: Static torque coefficient on the optimized rotor (Menet, 2001).....	23
Figure 11: Pressure Contours (Pa) on the Optimized Rotor ( $\Theta = 45$ degrees) (Menet, 2001).....	23
Figure 12: Active Yaw Controlled by Pressure Sensors at 13 and 15 (Enevoldsen, 2010).....	25
Figure 13: Passive Tail Vane Design (Kodric, 1989).....	26
Figure 14: Passive Tail Vane Design (Kuo, Hai P. 2011) .....	27
Figure 15: "Wind Shark" Tail Vane (Poole, 2007) .....	27
Figure 16: Final Turbine Assembly with Base .....	28
Figure 17: Shaft Endurance Limit Based on Torque Applied .....	30
Figure 18: Turbine Assembly Height to Width Ratio, shown in inches.....	33
Figure 19: Savonius Blade Notched for End Cap Construction .....	34
Figure 20: Enclosure and Tail Vane .....	35
Figure 21: Lower Shaft Assembly .....	38
Figure 22: Upper Shaft Assembly Exploded View .....	39
Figure 23: Four bladed VAWT initial design.....	40

Figure 24: Separator disk with engraved blade troughs.....	40
Figure 25: Cap feature to secure turbine assembly.....	41
Figure 26: Exploded view of turbine assembly .....	42
Figure 27: Base.....	43
Figure 28: Tail Vane Experimental Setup.....	45
Figure 29: Portable Electronic Spring Scale .....	46
Figure 30: Digital Laser Tachometer .....	47
Figure 31: Digital Anemometer.....	47
Figure 32: Torque at Low Wind Speed.....	48
Figure 33: Power at Low Wind Speed.....	49
Figure 34: Torque at High Wind Speed .....	49
Figure 35: Power at High Wind Speed .....	50
Figure 36: Tail Vane Alignment Reaction Speed .....	52
Figure 37: Funneling Experimental Setup.....	56
Figure 38: Torque Comparison of Funneling Setup .....	57
Figure 39: Power Comparison of Funneling Setup .....	57

## List of Tables

Table 1: Summary of Enclosure Validation Tests.....	7
Table 2: Performance of Savonius Turbine Designs (Saha, Thotla, & Maly, 2008) .....	19
Table 3: Blade feature coordinates for optimal shape (Mohamed, 2011) .....	20
Table 4: Mathematical Modeling Values Summary .....	32
Table 5: Blade and Enclosure Materials Matrix .....	36
Table 6: Tail Vane Material Design Matrix.....	37

## Introduction

Climate change is a heavily researched phenomenon that has been attributed to the increase of greenhouse gases. Energy production is the primary producer of greenhouse gases, specifically carbon dioxide, released into the atmosphere. Coal burning power plants are accountable for about 30% of the global carbon dioxide emission. Burning coal provides approximately 40% of the world's energy supply (Greenpeace, 2013). With an ever-increasing population and energy demand, coal power plants will inevitably grow in number if other forms of energy production do not replace it.

Wind power is a sustainable and renewable alternative energy source that contributes minimal carbon dioxide emissions into the atmosphere. Wind power generation is increasing by 30% annually; however, it was only responsible for 2.5% of global energy in 2010 (Kroldrup, 2010). Wind turbines are currently used in 83 countries to produce electricity. The most common turbine design used in wind farm applications is a horizontal axis wind turbine (HAWT). A vertical axis wind turbine (VAWT) design is an alternative design consisting of blades rotating around a vertical axle. There are two most widely used sub-categories of VAWTs that are defined by blade shape. Savonius blades feature a cup shape, catching the wind and advancing the blade using drag force. Darrieus blade designs use airfoils to create lift and rotate the turbine. HAWTs are more commercially produced because they are capable of generating more electricity at higher wind speeds. VAWTs are more feasible in rapidly varying wind direction because their design allows them to generate electricity regardless.

In an attempt to increase the coefficient of performance of VAWTs, a past Worcester Polytechnic Institute MQP group investigated the effects of partially enclosing the turbine to restrict airflow from striking the returning blades. It was demonstrated that an enclosure improved the turbine's angular velocity through small scale wind tunnel testing (Brandmaier, et al, 2013).

## Project Goal

The goal of this research was to design, build, and evaluate a Savonius VAWT prototype with the Brandmaier, et al, partial enclosure with the addition of a wind alignment device. The primary objective of the project is to show the proof of concept of a VAWT using an enclosure to increase the coefficient of performance. The secondary objective is to design an effective wind-direction that will keep the enclosure in the optimal position relative to the wind direction.

Understanding the effects of a simple enclosure on VAWT coefficient of performance may prove instrumental for creating a VAWT that is cost competitive with conventional, fossil fuel energy generation. Clean and renewable distributed energy generation will benefit from lower cost and more efficient VAWT design.



# Literature Review

## Savonius vs. Darrieus Blades

Savonius and Darrieus blades are the two main types of vertical axis wind turbine blades. The rotation of Darrieus turbines is dependent on lifting forces that develop as wind hits the airfoils. The rotation of Savonius turbines is dependent on drag forces that develop when the turbine blades cup the wind. The lifting forces of the Darrieus turbines cause large centrifugal forces, so the blades of these turbines must be strong. Since Darrieus turbines can rotate at a faster speed than the prevailing wind, these turbines are typically used to generate electricity. On the other hand, Savonius turbines rotate slower than the prevailing wind and generate larger torque outputs. This combination makes these turbines suitable for pumping water or grinding grain (Reuk, 2013).

## Optimal Rotor and Blade Design

Within Savonius style blades, there are a number of configurations that have been examined to increase the coefficient of performance of VAWTs. The coefficient of performance,  $C_p$ , is defined as

$$C_p = \frac{P_s}{P}$$

where  $P$  is the power of an airstream with a mass flow rate moving through a defined area calculated with the equation

$$P = \rho A V \frac{1}{2} V^2 = \frac{1}{2} \rho A V^3$$

where  $\rho$  is the density of the air,  $A$  is the swept area of the blades and  $V$  is the velocity of the air.  $P_s$  is the power of the turbine shaft is calculated with experimentally measured brake torque and angular velocity.

Modifying the cup shape, adding gaps for vortices at the central axis, and helical blades are common improvements to the basic Savonius shape.

The aspect ratio of the VAWT is given by the height of the turbine divided by the diameter of the turbine blades. The typical aspect ratio of VAWTs is 1.5, meaning the height should be 1.5 times greater than the diameter of a VAWT (Paraschivoiu, 2002).

Saha et al. (2008), developed optimal parameter combinations for Savonius VAWTs. They investigated how the coefficient of performance changes with respect to the number of stages, number of blades, and blade shape. Experiments in this study tested 14 total combinations of stages (1-3), number of blades (2-4), and blade shape, (semicircular or twisted). Stages refer to separated levels of the turbine containing their own blades as seen in Figure 5.

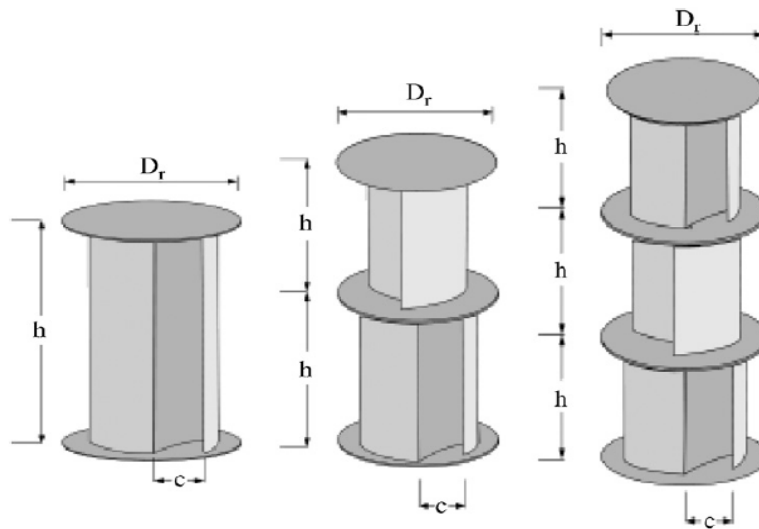


Figure 5: VAWT Turbines with Varying Stages (Saha et al., 2008)

The tests were run in a wind tunnel at wind velocities ranging from 6 - 11 m/s. Wind velocity was measured with a thermal velocity probe anemometer, and static and dynamic torques were measured with a brake dynamometer (Saha et al., 2008).

The researchers concluded that all varying design elements tested had an individual impact on the turbines' coefficient of performance, and combinations of the different design elements increased or decreased the coefficient of performance even further. Experimental studies discovered that when the number of stages is increased from one to two, the turbine performs more efficiently. Further

increasing the number of stages from two to three reduces the coefficient of performance due to the increased rotor inertia (Saha et al., 2008).

Blade design was experimentally tested in conjunction with the number of stages. A semicircular blade (twist =  $0^\circ$  degrees) and a twisted blade (twist =  $12.5^\circ$  degrees) were the two variations tested. The twisted blade outperformed the semicircular blade in all levels of stages (1-3). Exact value differences can be seen in Table 1. With a twisted blade, the maximum force migrates and acts at the tip of the blade, instead of centrally in the case of the semicircular blade. A longer moment arm for the twisted blade increases the torque created leading to a higher coefficient of performance (Saha et al., 2008).

Another variation investigated was the effect of increasing the number of blades from two to three. In all stage variations, the increase in blades reduced the turbine's coefficient of performance. Three-bladed systems performed worse in all tests comparatively to two-bladed systems. This was associated this decrease in performance to additional wind turbulence. When wind is captured by the advancing blade, some is reflected back and contacts the returning blade. With three blades, there is less space between each advancing and returning blade, increasing the negative effects of this phenomenon (Saha et al., 2008).

All the results gathered by the investigators were organized into a table expressing the varying design combinations and their respective experimental characteristics. Table 2 shown below from the publication shows the results of the investigation.

Table 2: Performance of Savonius Turbine Designs (Saha, Thotla, & Malty, 2008)

Rotor system	No. of blades	Blade shape	Blade height (m)	Blade chord (m)	Aspect ratio	Projected area (m <sup>2</sup> )	Free stream velocity (m/s)	Max. power coefficient (C <sub>p</sub> )
Single-stage	2	Semicircular	0.173	0.109	1.58	0.0377	8.23	0.18
		Twisted						0.19
	3	Semicircular						0.15
		Twisted						0.16
Two-stage	2	Semicircular	0.122	0.077	1.58	0.0377	7.30	0.29
		Twisted						0.31
	3	Semicircular						0.26
		Twisted						0.28
Three-stage	2	Semicircular	0.100	0.063	1.58	0.0377	8.23	0.23
		Twisted						0.24
	3	Semicircular						0.20
		Twisted						0.21

Islam et al. (2005) tested the impact two, three, and four blade rotors have on the normal drag coefficient, tangential drag coefficient, and torque coefficient. Their results showed that as the number of blades increased, there was no significant change in drag coefficient or net output torque. Their studies also showed that as the number of blades increased, the starting torque increases (Islam et al., 2005). These results further proved that a two bladed rotor is the best option for the design.

Mohamed et al. (2011), showed how to modify a semicircular blade to catch the wind more effectively. Figure 6 shows a traditional Savonius set of blades.

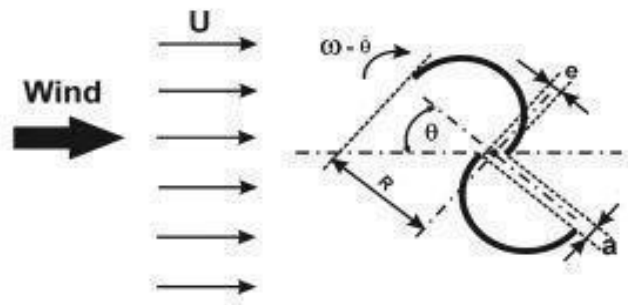


Figure 6: Traditional Savonius blades (Mohamed, Janiga, Pap, & Thevenin, 2010)

For the duration of their trials, fixed distances were used for the parameters  $e$  and  $a$ , which were equal to  $0$  and  $R/3$ , respectively. It is also important to note that in this study, a shield was used to

limit the wind that hits the returning blade (Mohamed et al., 2011). Since an enclosure was used to perform the same task, it can be assumed that the results from this study are applicable to the current VAWT enclosure design.

Figure 7 shows where the three variable points are located on the blade. Each coordinate is divided by the radius of the blade, and these values must fall in the corresponding ranges that are given in Table 3 to achieve the optimal blade shape (Mohamed et al., 2011).

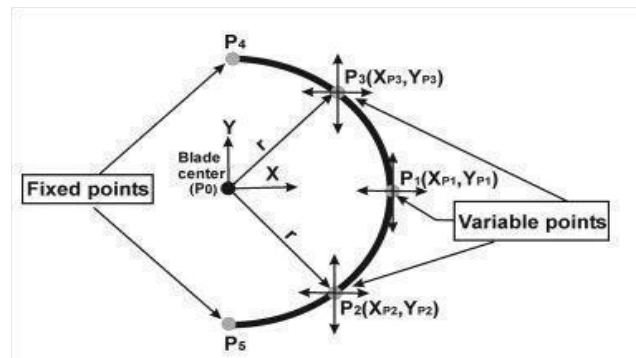


Figure 7: Savonius Blade Optimization (Mohamed, 2011)

Parameter	Minimum allowed	Maximum allowed
$X_{P1}/r$	0.53	1.47
$Y_{P1}/r$	-0.24	0.24
$X_{P2}/r$	0.24	1.2
$Y_{P2}/r$	-0.94	-0.24
$X_{P3}/r$	0.24	1.2
$Y_{P3}/r$	0.24	0.94

Table 3: Blade feature coordinates for optimal shape (Mohamed, 2011)

To test how the modified shape performs against traditional Savonius blades, the tip-speed ratio

is compared to the torque coefficient and the coefficient of performance for three scenarios. The scenarios included in the graphical analysis are; traditional Savonius blades without the obstacle discussed in the past study, traditional Savonius blades with the obstacle, and the optimally shaped Savonius blades with the obstacle. The graphical analysis can be seen in Figure 8, and it shows that the optimally shaped blade yields a tip-speed ratio ( $\lambda$ ) than the traditionally shaped blade (Mohamed et al., 2011).  $\lambda$  is defined as

$$\lambda = \frac{\omega D}{2V}$$

where  $\omega$  is the angular velocity of the turbine,  $D$  is the diameter of the turbine, and  $V$  is the wind velocity.

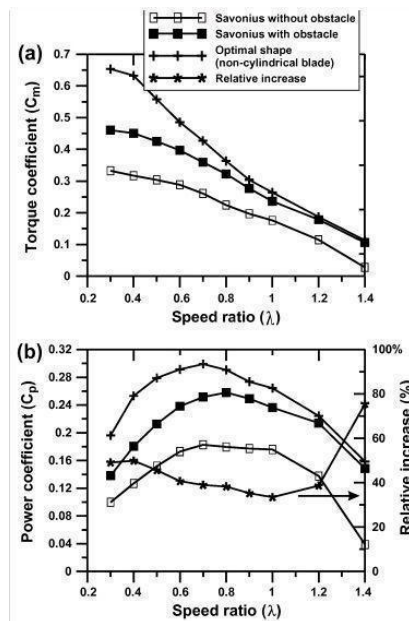


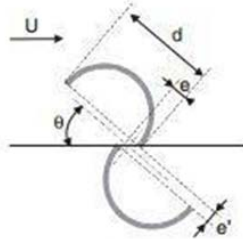
Figure 8: Optimum Savonius Blade Comparison (Mohamed, 2011)

L.J. Menet conducted a study that focused on the optimal orientation of Savonius blades. He proposed that the blades should not be directly aligned with each other. In this study, Menet tested how rotating one of the blades toward the second blade would affect the static torque of the rotor. This

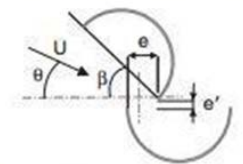
modified orientation is depicted in Figure 9 below.



**Fig. 43.1.** 3D representation



**Fig. 43.2.** Savonius rotor



**Fig. 43.3.** Modified rotor

**Figure 9: Modified Savonius Rotor (Menet, 2001)**

Menet conducted static flow simulation experiments that compared the modified Savonius rotor with the traditional Savonius rotor, and concluded that the modified rotor maximizes static torque. These results are shown in Figure 10.

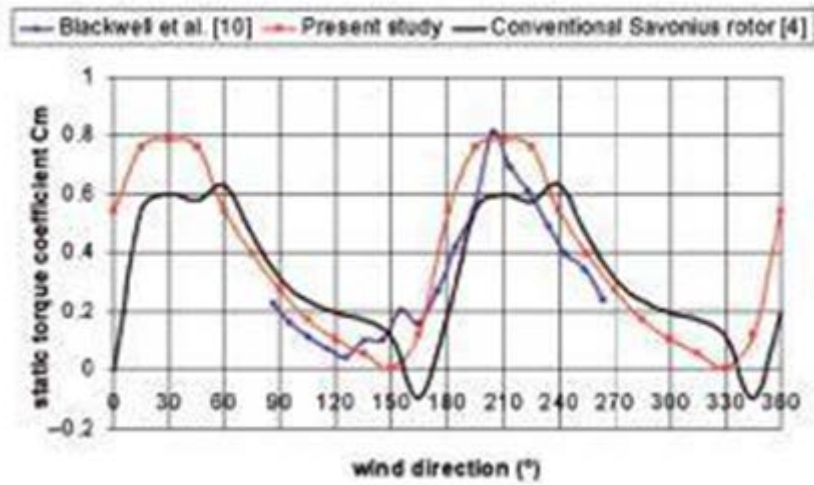


Figure 10: Static torque coefficient on the optimized rotor (Menet, 2001)

Moreover, Menet concluded that there is an increase in pressure in the cupped area of the modified rotor. The pressure contours of the two different rotors can be seen in Figure 11. Menet determined that the optimal orientation to maximize static torque is when  $\beta = 55^\circ$  (Menet, 2001).

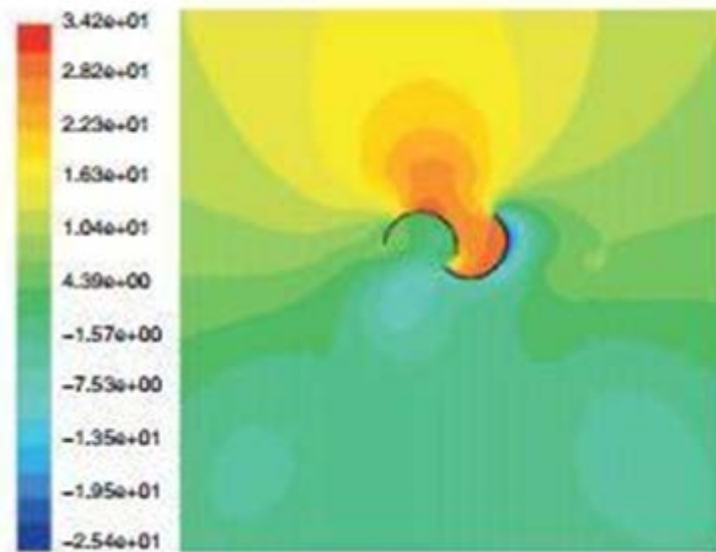


Figure 11: Pressure Contours (Pa) on the Optimized Rotor ( $\Theta = 45$  degrees) (Menet, 2001)

## Enclosure

There is limited research on the effect of enclosures or obstacles on the performance on VAWTs.



Some results showed that an enclosure could significantly increase its coefficient of power ( $C_p$ ) and torque coefficient ( $C_m$ ). Wind pushes both forward and against the rotor blades during its rotation, so efforts to minimize wind flow onto the blades in the returning direction would theoretically increase performance. A typical VAWT with Savonius rotor blades experiences wind in both directions, and spins only because of the difference in drag coefficients of the blades as the angle of attack changes. An enclosure or an obstacle could reduce the wind flowing into the returning blades and increase the flow speed flowing into the advancing blade (Mohamed, 2010).

Researchers at University of Magdeburg in Germany conducted a study on the placement of a flat plate that reduces the oncoming wind in front of the return blade of the VAWT. They found that an obstacle with approximately a  $100^\circ$  degree angle was the optimal value for two-blade Savonius turbine, given their specific testing geometry. With this set up, the torque coefficient ( $C_m$ ) increased from 0.33 to 0.46 and the coefficient of performance increased 30 percent at speed ratio of 0.3 (Mohamed, 2010). On average, Savonius shaped blades have a coefficient of performance of 0.15-0.3 (Wortman, 1983). The effect from an obstacle had a significant numerical result on improving the coefficient of performance. Based on this research, an enclosure was added on our wind turbine.

A design proposed by Letcher used a nozzle to increase the velocity of wind going into the advancing blade and deflecting the wind entering to the returning blade. Again, the research shows an increase in coefficient of performance due to reductions in the negatively-affecting side of the turbine area. The researchers noted clearly that use of a nozzle, while increasing efficiency, poses implementation issues with sites that have more than one prevailing wind direction (Letcher, 2010).

## Alignment Methods

To ensure that the benefits of the enclosure will be realized, it must be in the optimal position, which changes with varying wind direction. If the enclosure is angled incorrectly, it may block all the wind from the turbine and inhibit power generation. There are a number of alignment methods used in

vertical and horizontal wind turbines, and they fall into categories of either active or passive systems.

An active alignment system senses the wind direction, and uses powered motion to rotate, or yaw, into the wind. These active systems typically use pressure sensors, wind vanes, or anemometers. By mounting a pressure sensor on each side of the wind turbine, and comparing their readouts simultaneously, the system can infer which direction to rotate. When the pressures are equal, the turbine is perfectly aligned with the wind (Enevoldsen, Frydendal, Poulsen, & Rubak, 2010). Figure 12, shows a HAWT diagram with pressure sensors, labeled 13 and 15.

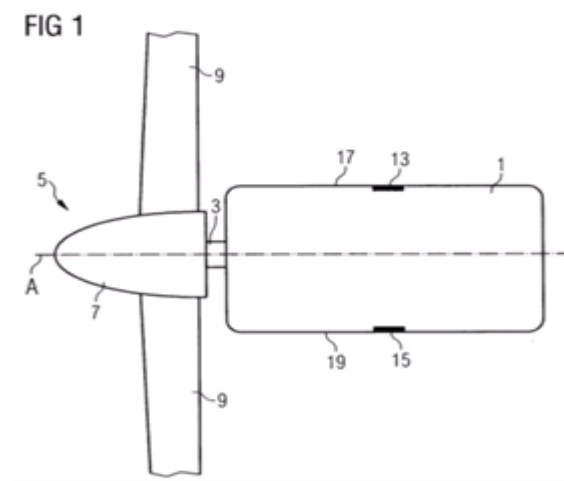


Figure 12: Active Yaw Controlled by Pressure Sensors at 13 and 15 (Enevoldsen, 2010)

A wind vane can be used in conjunction with a potentiometer and yaw gear. The wind vane detects the direction of the wind and the potentiometer converts this linear motion into a change in resistance. The change in resistance can then control the yaw drive (Elliot, 2001). An anemometer can be used to record wind speeds and directions. These recordings control the yaw drive and it will rotate into optimal position. An ultrasonic anemometer detects speed variations in pulses of ultrasonic waves to infer wind direction and velocity. Active alignment options allow precise adjustments and easier integration of disaster-condition operations. As such, they are standard for high-output HAWTs.

The simplest passive system utilizes a tail vane to align the turbine into the wind. When not aligned, wind hits the surface of the vane and creates an unbalanced moment about the central axis,

which turns the turbine until the angle at which the wind hits the vane becomes zero. There are two major design choices with this system, shape and placement. There are many patents and patent applications for tail vane designs. Some tail vane examples are depicted below, which display the wide variety of shapes that can function as a tail vane. Figure 13 is a design that is similar to the tail of an airplane, and Figure 14 shows a wind turbine with a simple tail vane similar to that of a weather vane. The tail vane shown in Figure 15 is a component of a VAWT called the “Wind Shark Vertical Turbine.” It is critical that the rotation caused by the tail vane is stronger than the moment incurred by the asymmetrical shape of the enclosure itself in all these examples, as well as our design.

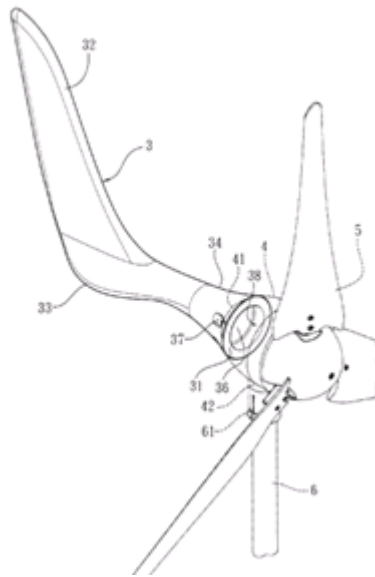


Figure 13: Passive Tail Vane Design (Kodric, 1989)

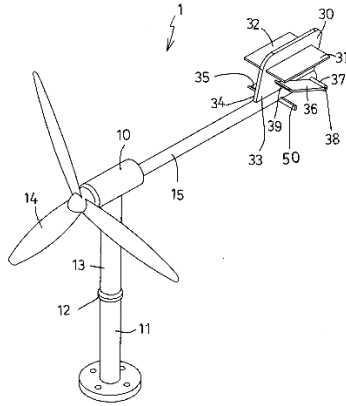


Figure 14: Passive Tail Vane Design (Kuo, Hai P. 2011)

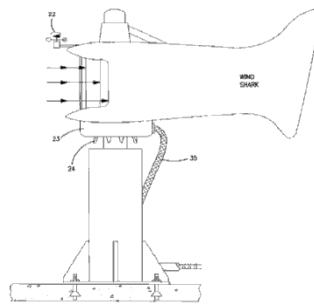


FIG. 8

Figure 15: "Wind Shark" Tail Vane (Poole, 2007)

In addition to the shape, the location of the fin must also be assessed. The tail vane could be mounted above, in-line, or below the swept area of the VAWT. If the vane is offset, either above or below the enclosure, changing wind direction would also induce a pitch or roll moment, pressing the turbine's central axis off of perfectly vertical. However, in an installation with many turbines, it may be advantageous to mount the tail vane outside the swept area, as it would reduce the turbulence of the wind.

## Design Overview

Based on the literature review and the design calculations found in Appendix A, the following design was chosen to be constructed and tested. A number of components underwent design iterations throughout the process as a result of either refined literary evidence that supported a specific design feature, or manufacturing and assembly challenges. To summarize and defend the proposed prototype, a number of design choices are reviewed below that influenced the prototype as it is presented. Figure 16 shows the final design of our VAWT prototype and constructed base.

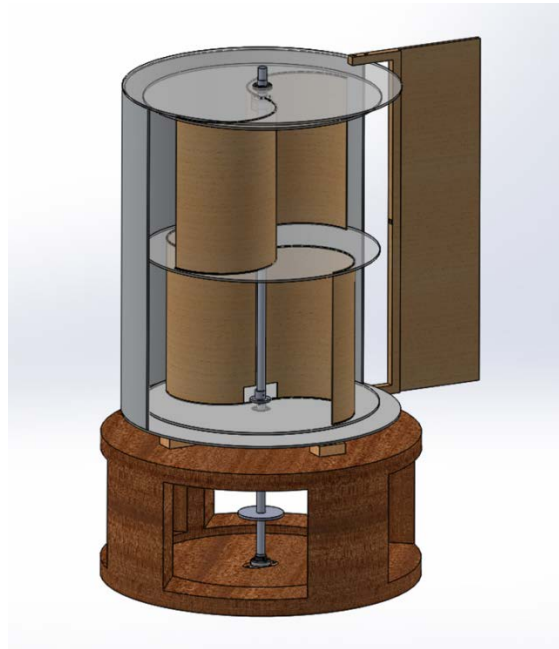


Figure 16: Final Turbine Assembly with Base

## Mathematical Modeling

The turbine's performance was calculated using some basic formulae regarding forces and torque. For this and all calculations shown in full, see Appendix A.

$$\text{Power} = \frac{1}{2} * \rho * V^3 * A * c_p$$

Where  $\rho$  is the density of air,  $V$  is the mean velocity of the wind,  $A$  is the swept area (front facing), and  $c_p$  is the estimated coefficient of performance of the turbine. The coefficient of performance was assumed using similar turbines whose coefficient was found experimentally. Values for this and all calculations are summarized below in Table 3. Torque applied to the shaft is found by:

$$T = \frac{\text{Power}}{\text{Angular Velocity}}$$

where

$$\text{Angular Velocity} = \frac{V}{t * r}$$

and

$$t = \frac{\text{Wind Velocity}}{\text{Blade Tip Linear Velocity}} = \frac{V_{\text{Wind}}}{V_{\text{Blade}}}$$

$t$  is the tip speed ratio of the blades, and  $r$  is the radius of the blades. The tip speed ratio was found experimentally. The literature review shows an optimal tip speed ratio of 0.8, which we aimed to achieve.

The allowable torque stress on the shaft was estimated using the equation:

$$N = \frac{S_y}{\tau_{\max}}$$

where  $N$  is the safety factor,  $S_y$  is the yield strength, and  $\tau_{\max}$  is the maximum shear stresses.  $\tau_{\max}$  was found using the formula:

$$\tau_{\max} = \frac{T * r}{2 * I}$$

where  $T$  is the torque applied,  $r$  is the radius of the shaft, and  $I$  is the area moment of inertia of the

shaft. Note that the maximum torque is different than the value used in the power equation above. The endurance limit based on the torque stress in the shaft is shown in Figure 17.

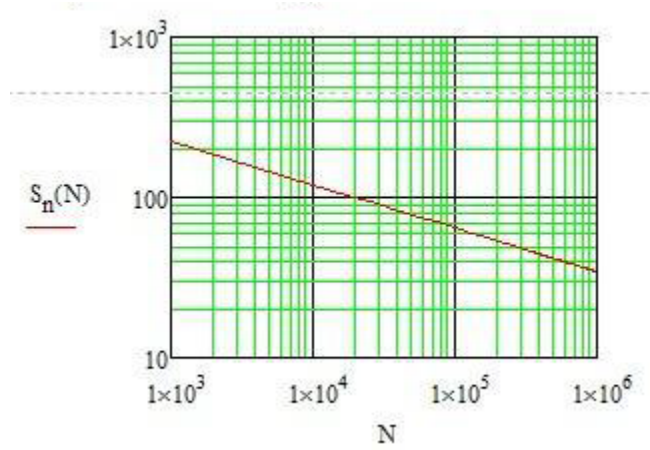


Figure 17: Shaft Endurance Limit Based on Torque Applied

Where  $S_n(N)$  is the fatigue strength at a given  $N$  cycles, and is calculated using the endurance limit of the material and correction factors for load, size, surface finish, temperature, and reliability.

Shaft deflection due to wind load on the enclosure was estimated using a linear wind distribution across a spherical object with a diameter of the enclosure, and the moment of inertia incurred by the weight of the tail vane. A spherical object was used as a broad approximation as an object similar in shape to the shaft.  $Y$ , deflection is defined as:

$$y_{\max} = \frac{1}{E * I} * \left( \frac{-M_1 * l^2}{2} + \frac{R_1}{6} * l^3 - \frac{M_{\text{vane}}}{2} l^2 - \frac{w}{24} * (l - 1)^4 \right)$$

$E$  is the young's Modulus of the material,  $I$  is the area moment of inertia,  $M_1$  is the moment incurred by the wind load,  $l$  is the length of the shaft,  $R_1$  is the supporting force at the base,  $M_{\text{vane}}$  is the moment incurred by the weight of the tail vane, and  $w$  is the force of the wind on the object.

The estimation of the failure of the blade due to wind load is modeled after a thin-walled

pressure vessel. The longitudinal and tangential stresses are:

$$\sigma_L = \frac{p * r}{2 * t}$$

$$\sigma_T = \frac{p * r}{t}$$

Where p is the pressure due to wind, r is the radius of the blade, and t is the thickness of the blade. These two are combined into a von Mises stress,  $\sigma'$ , and compared to the yield strength of the material,  $S_y$ , below:

$$N = \frac{S_y}{\sigma'}$$

The stresses on the tail vane are calculated using a concentrated force on the centroid of the tail vane action on a moment on the shaft. These are combined using von Mises theory, similar to above, and examined both at the base, and at the tail vane mount, which experience different stresses due to their different material and area.

The acceleration of the enclosure is given by the formula:

$$\alpha = \frac{\tau}{I}$$

Where  $\tau$  is the torque applied to the tail vane by the wind and I is the area moment of inertia of the tail vane and enclosure. Time to rotate from initial to final position is found by the equation:

$$t = \left( \frac{\theta}{.5 * \alpha} \right)^{.5}$$



Table 4: Mathematical Modeling Values Summary

Key Property	Value	Unit
Power	.16	Watts
Torque	.03	Newton Meters
Angular Velocity	48	Revolutions per minute
Tip Speed Ratio	.98	
Safety Factor	11.5	
Maximum Allowable Torque	$1.1 \times 10^7$	Newton Meters
Maximum Deflection	11.2	Millimeters

It is important to understand that these key values were the mathematic approximations of the turbine that were used to determine its geometry as-built. To clarify, the power in the table above is not the target maximum power of the turbine, but rather the power at the wind speed that we expected to be able to test. The true performance of the turbine was not known until after the testing methodology was completed.

## Size and Geometry

The size of the prototype was confined by a number of design criteria. Primarily, it needed to be large enough to demonstrate the principles of the enclosure and wind-alignment device compared to the prototype with the enclosure and alignment device removed. This means it must be large enough to harvest wind in the design environment, rather than a wind tunnel. Additionally, the prototype should reflect a marketable product, since this is the next step in a commercialization process. A prototype that is approximately the same size as a viable product will be more useful for answering questions about manufacturing, expected power generation, and marketability. Another constraint is the budget of the

prototype project. This limits the size and material complexity of the prototype considerably, as a number of materials needed to be purchased and manufactured in order to test the design.

The specific geometry of the turbine was defined through basic calculations of operation at desired wind speeds. The optimal aspect ratio, height to width, of the turbine is discussed by Paraschivoiu in the literature review, and as a result was closely set to 1.5 shown in Figure 18.

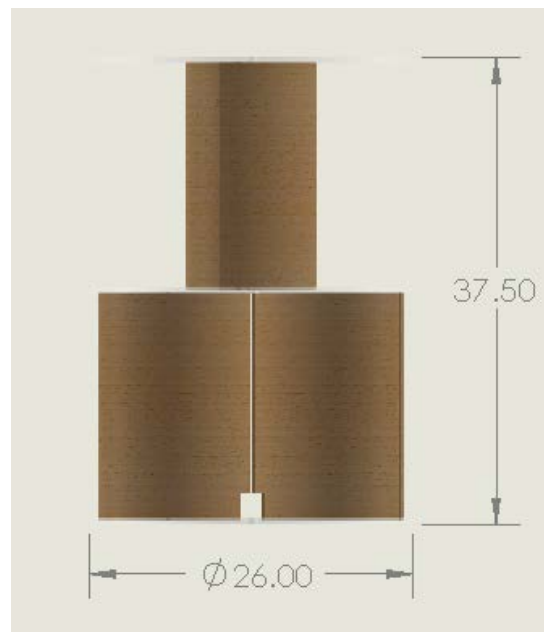


Figure 18: Turbine Assembly Height to Width Ratio, shown in inches

## Blades

The concept and previous tests of the VAWT enclosure by Brandmaier, et al, was all conducted using drag-type turbine blades. While it may be possible to use an enclosure with lift-style blades like an H-rotor or Darrieus blades, it was decided to continue testing drag-type turbine blades for the enclosure concept. Given the expected marketable size of a VAWT with an enclosure, it will likely be performing in low- or no-wind conditions for the majority of the time. In light of this, it is fitting to use a drag-type blade that can be self-starting.

The blade shapes of Savonius VAWTs are under constant improvement. When selecting the blade shape, a balance between performance, cost, and ease of manufacture were the priorities. To accomplish this, classic Savonius-profile blades in a two-stage turbine were chosen, as demonstrated by Saha, et al, in the literature review. This combination best suited the need for a design that had a high coefficient of performance and manufacturability. As Saha, et al, determined the design choices that yielded the largest coefficient of performance were: two blades rather than three, a two stage turbine rather than a one or three stage, and blades with a 12.5 degree twist. The increase in the coefficient of performance from one stage to two, using semicircular blades, is 0.18 to 0.29. The coefficient of performance for a two blade, two stage design with semicircular blades is 0.29. Adding a 12.5 degree twist to the blade would marginally increase the coefficient of performance to 0.31, which was not done to save manufacturing time. Lastly, a method of fixing the turbine to the axle was determined, and the blades were modified to accommodate the end cap (Figure 25) with a notch, displayed in Figure 19.



**Figure 19: Savonius Blade Notched for End Cap Construction**

## Enclosure and Wind-Alignment Device

The enclosure that was tested in the prototype was the selected design from Brandmaier, et al., (2013). Their geometry will be replicated, and the appropriate gap between the turbine and enclosure was assumed to be 2 inches. This dimension was not recorded by Brandmaier, et al.

After reviewing the literature, a passive wind-alignment device was chosen as the best fit for the prototype. The enclosure will be lightweight and its center of gravity will be nearly concentric with the center of the shaft, so only a small moment is needed to turn the enclosure. Active systems need additional electronics and their associated cost exceeded the available budget. The tail vane concept was chosen as the best means to control yaw for the wind-alignment device. After reviewing the forces on the system, it was decided that the tail vane should be mounted in same horizontal plane as the enclosure, rather than above or below, to avoid introducing additional roll or pitch to the shaft and system. After design iterations and calculation of the effect of the tail vane size on a number of parameters included in Appendix A, the proposed design was selected, shown below in Figure 20.

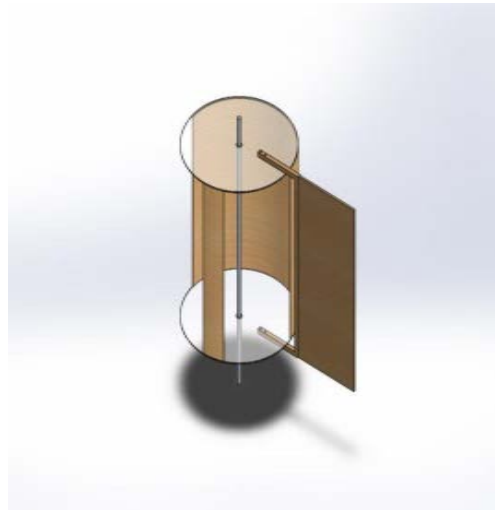


Figure 20: Enclosure and Tail Vane

## Materials

Two design matrices were developed, Tables 5 and 6, to determine what the best material option was for the enclosure, blades, and tail vane. The enclosure and blade materials were combined in one matrix because these structures need to withstand similar pressures and forces and perform similar tasks. Both structures needed to withstand the pressure caused by the “sandwich” assembly, they could not break due to the force of wind, they could rotate with the wind, and they were both semicircular structures.

**Table 5: Blade and Enclosure Materials Matrix**

Enclosure/Blades	Cost	Strength	Density	Availability	Manufacturability	Rank
Weighing Factor	.3	.1	.1	.3	.2	
Fiberglass	3 .9	8 .8	4 .4	9 2.7	2 .4	5.2
Rocket body tube	2 .6	8 .8	5 .5	1 .3	5 1	3.2
Postal Tube	7 2.1	4 .4	8 .8	1 .3	7 1.4	5.0
Sonotube	9 2.7	5 .5	8 .8	9 2.7	7 1.4	8.1
Aluminum Sheet Metal	6 1.8	7 .7	2 .2	9 2.7	6 1.2	6.6
Divinycell	4 1.2	3 .3	9 .9	9 2.7	3 .6	5.7
Owen's Corning Foam *Blades only	7 2.1	2 .2	7 .7	9 2.7	4 .8	6.5

For both matrices, the design parameters were cost, strength, density, availability, and manufacturability. In the first matrix (blades and enclosure), cost and availability were weighted the highest. This was because the budget was limited and materials had to be readily available to be considered a viable option. The parameter that was weighted the next highest was manufacturability. Due to time and machinery constraints, some of the material's complex manufacturing processes were deemed less viable. The density and strength of the enclosures were weighted the least. The strength of

the blades is not as important for this application because the project only examined a prototype tested in lower winds. The density was also listed as having lower importance because the structures supporting the blades and enclosures could be made stronger to support a denser part, even though less dense was preferred. Based on this matrix, the sonotube was concluded to be the best material choice for the blades.

**Table 6: Tail Vane Material Design Matrix**

	Cost	Strength	Weight	Availability	Manufacturability	Rank
Weighing Factor	.275	.15	.275	.05	.25	
Triple Wall Cardboard	8 2.2	4 .45	8 2.2	9 .45	9 2.25	7.55
Thin Plywood	7 1.925	3 .6	7 1.925	9 .45	8 2	6.9
Beech Wood	3 .825	5 .75	5 1.375	9 .45	7 1.75	5.15
Acrylic	4 1.1	6 .9	4 1.1	9 .45	6 1.5	5.05
Aluminum Sheet Metal	5 1.375	7 1.05	2 .55	9 .45	6 1.5	4.925
Owen's Corning Foam	4 1.1	2 .3	9 2.475	9 .45	5 1.25	5.575

The design matrix for the enclosure and tail vane included the same design parameters as the previous matrix. However, they are weighted differently. Cost and density are weighted the highest. As mentioned before, cost was a high priority due to financial constraints. Since the tail vane would be attached to the side of the enclosure, it was important that it was as light as possible to reduce unwanted shaft deflection and rotational inertia. Manufacturability was the next highest weighted parameter. Time and machinery constraints forced some material options to be less viable than others. The design parameter that was weighted the next highest was the strength. It was important that the material was strong enough to withstand the forces due to the wind. The parameter with the lowest weight was availability. Although availability is important, all of the materials listed in this matrix were

readily available.

For this tail vane matrix, low cost, low density, high strength, high availability, and quick and easy manufacturability received high ranks. The reasoning for this corresponds with the reasoning previously discussed. Based on this matrix, triple-wall cardboard should be used for the tail vane. While cardboard was shown to rank higher for the enclosure as well, sheet metal was later chosen due to its ease of assembly. All of the specific information regarding the parameters can be found in Appendix B.

## Assembly

The prototype was comprised of two distinct sub-assemblies, the turbine and enclosure, and their respective fasteners and bearings, and the downstream components, the gearbox and motor. The enclosure subassembly was supported by four ball transfer rollers mounted on the base, which act as one large thrust bearing. This carried the load of the enclosure and allowed it to rotate about the shaft independently. The turbine assembly was fixed to the shaft using two end caps, and rested on the enclosure using another thrust bearing, not exploded in the view. This thrust bearing between the turbine and enclosure supported the weight of the shaft, gear, and turbine assembly, as shown below in Figure 21.

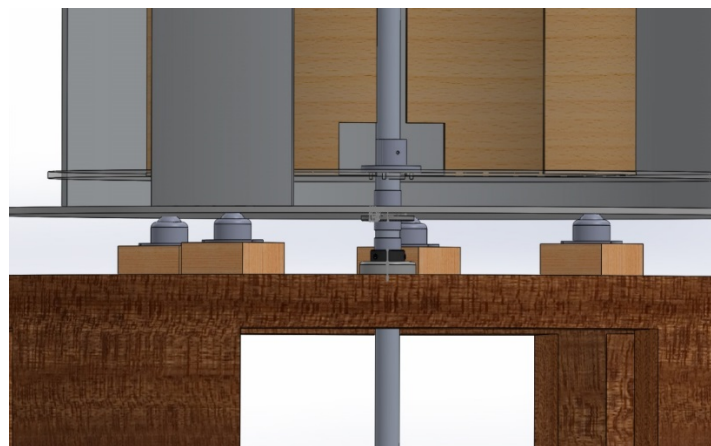


Figure 21: Lower Shaft Assembly

The upper section of the shaft can be seen below in Figure 22. The enclosure top disk, G, was

mated to the shaft, E, using a radial bearing, F. This radial bearing helped to keep the enclosure concentric with the turbine shaft. The turbine subassembly was fixed to the shaft using two end caps, one of which is seen here at H. The end caps secured to the upper and lower acrylic plates, and to the shaft using set screws.

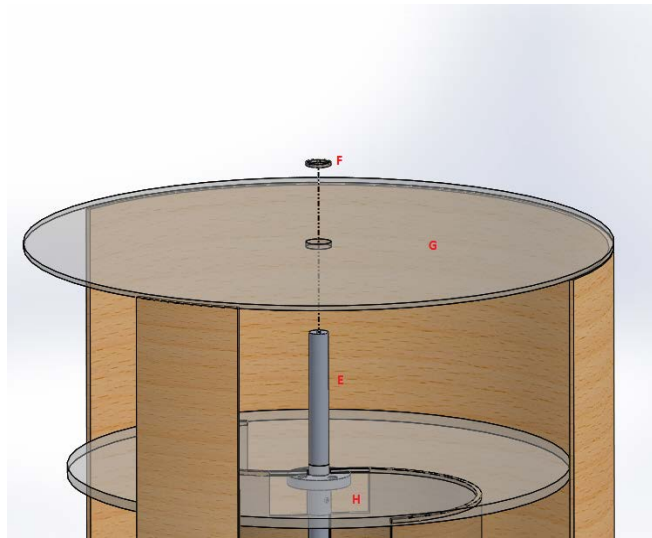


Figure 22: Upper Shaft Assembly Exploded View

## Design Iterations

The design underwent a number of iterations as the component assembly was visualized and the potential difficulties it presented. These iterations involved adapting materials selection as well as part geometries to minimize assembly challenges. As new literary sources were acquired and understood, the prototype was adapted accordingly to optimize the design. Brandmaier, et al, used rectangular flat blades for ease of manufacturing. The blade design was changed despite the manufacturing benefits and selected Savonius type blades because of their capability to increase the coefficient of performance the turbine, as described in our literary review. Originally, the prototype only included one stage with four Savonius blades shown in Figure 23 below.



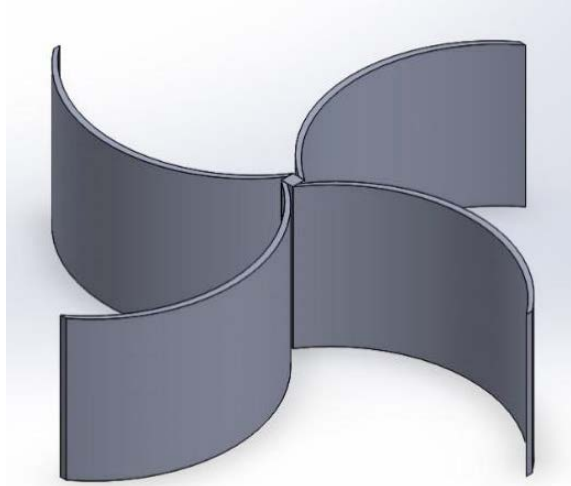


Figure 23: Four bladed VAWT initial design

After the investigation of Savonius turbine systems by Saha, et al, a two stage turbine was selected and the number of blades per stage was reduced to two. Ease of manufacturability was also a main concern in the design aspect of the turbine system. In an earlier design, each blade attached to the axle. These blades would have been far more difficult to manufacture, so an alternative was explored and implemented. In the present design, troughs are cut into the separating stages of the turbine for the blades to be attached with a press fit, displayed in Figure 24. This “sandwich” construction added rigidity to the turbine assembly by removing a cantilever load, and reduced the complexity of the blade design for mating to the turbine subassembly.

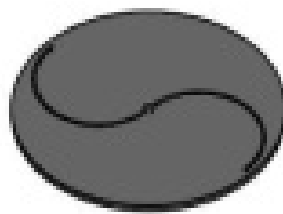


Figure 24: Separator disk with engraved blade troughs

## Turbine

The turbine section was assembled using the “sandwich construction” described above. The blades were constructed of sonotube, in accordance with the materials design matrix mentioned previously. The two stages of Savonius blades were separated by acrylic plates at the top, center, and bottom. A trough was cut on these plates, into which the blades were press fit and secured with epoxy. The plates all have a concentric hole at the center for the axle to pass through. Once assembled, the two-stage blade section was mated to the axle using end caps, shown below in Figure 25.



Figure 25: Cap feature to secure turbine assembly

This component has a through hole to mate to the axle, and four holes to mate to the respective enclosure plate. An exploded view of turbine assembly is shown here in Figure 26.

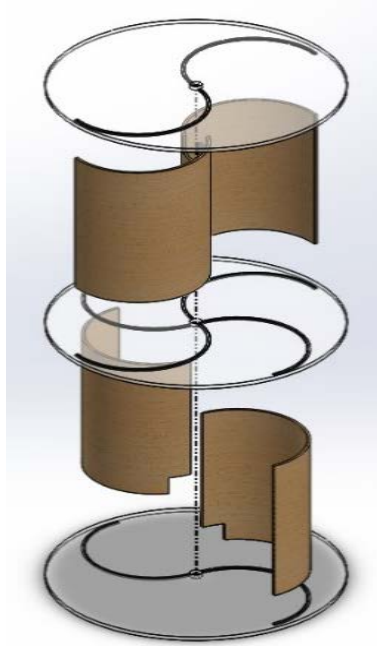


Figure 26: Exploded view of turbine assembly

## Enclosure and Tail Vane

The enclosure and tail vane attached only to the drive axle of the prototype. Press-fit bearings were used to mate the axle to the enclosure plates on the top and bottom of the enclosure. The weight of the enclosure and tail vane was supported by the pseudo thrust bearing design on the base. Not only did this support the weight of the subassembly, but it also allowed the enclosure and tail vane to rotate independently of the shaft, and maintain a greater range of center of gravity in the wind. The mounting bracket for the tail vane was manufactured to mates the enclosure disk to the tail vane. The enclosure was made of aluminum sheet metal. Although this material choice adds weight to the design, the ease of manufacturability with machinery found on WPI's campus made it a better selection. The tail vane supports were mounted to the enclosure mounting bracket, and served to transfer the force from the tail vane to the enclosure to rotate it when the wind changes direction. The tail vane was constructed of cardboard, as chosen in the tail vane design material matrix.

## Base and Downstream Mechanical Components

The base was designed in order to support the weight of the turbine, enclosure, and tail vane assembly, and house beneath it the motor and downstream components. The height of the base was determined to allow the motor to stand lengthwise, aligning the motor axle and the turbine axle in parallel. Having the axles oriented in parallel allowed for simpler power transmission. The width was determined to be wider than the turbine assembly to provide stabilization. Mounted on the top face of the base were the four ball transfer rollers that act as a thrust bearing for the enclosure to spin on. A flanged mounted ball bearing was attached to the center of the top and bottom of the base to orient the shaft and enable rotation. The final design for the base is displayed below in Figure 27.



Figure 27: Base

## Methodology

After construction of the turbine, base, and enclosure, various experimental tests were designed and conducted with the purpose of quantifying the torque output of the VAWT. A large floor fan provided constant wind speed for all torque and power experimental tests. The wind speed generated from the fan was controlled with the “high” and “low” governor on the fan, which produced average wind speeds of 3.7 m/s and 2.0 m/s, respectively. These speeds were measured across the swept area of the blades.

Torque and power experimental tests consisted of 4 individual circumstances; high and low fan speeds with and without the enclosure attached to the turbine system. The coefficient of performance of the system was measured using a brake dynamometer. This device consisted of a strap looped around a pulley on the shaft of the turbine with an electronic spring scale attached to each end. A load was applied with the strap to provide a torque against the rotation of the shaft. The electronic spring scales measured the tension applied on each end of the strap. By measuring the turbine angular velocity over increasing torques applied by the brake dynamometer, a power curve can be generated.

First, the fan was set to the desired selection (high or low) and angular velocity of the turbine were measured and recorded with no load. The brake dynamometer was then attached and the turbine angular velocity were again measured and recorded, along with the two force readings on the spring scales. The second data point recorded was the brake dynamometer attached with no additional tensional load. Subsequent data points were recorded with increasing tensional force applied to the brake dynamometer, at increments of approximately 0.1 lbs. Data recording continued with the increasing increments until the brake dynamometer applied enough torque to

the shaft to stall the turbine.

Another set of independent experimental tests were designed to quantify the rotational influence of the tail vane on the enclosure system. A series of tests that measured the time elapsed as the enclosure and tail vane return to the correct orientation after being initially set at an offset position. This test was conducted at  $45^\circ$ ,  $90^\circ$ ,  $135^\circ$ ,  $180^\circ$ ,  $-135^\circ$ ,  $-90^\circ$ , and  $-45^\circ$  degrees offset from the correct orientation. These offset angles and a detailed illustration of the experimental setup are shown in Figure 28 below.

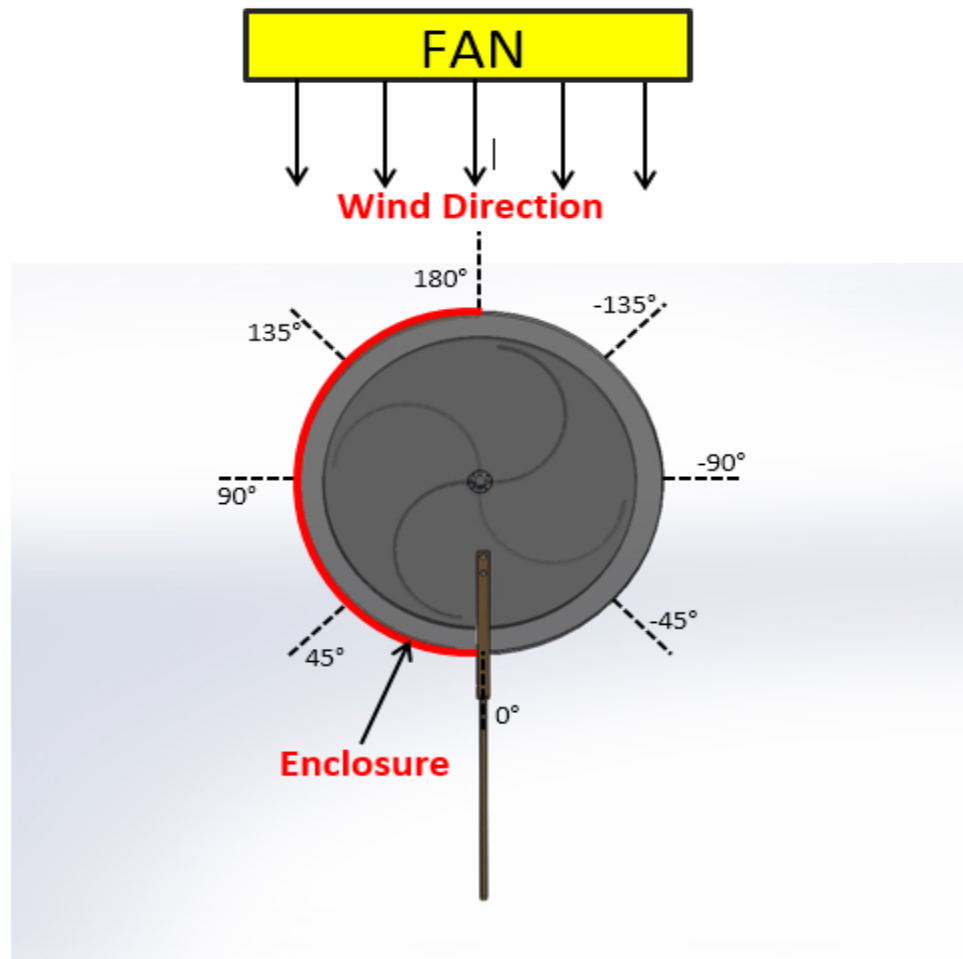


Figure 28: Tail Vane Experimental Setup

The fan blade speed was set to the high on the governor, providing the same 3.7 m/s average wind speed across the swept area of the turbine. The tail vane was set each test to an initial position of increasing multiples of 45°. The tail vane was then released, and elapsed time was recorded as the tail vane rotated the enclosure system to the correct orientation.

Equipment selection for all of the experimental testing was primarily driven by availability at facilities on WPI's campus and budget limitations. The main component of the brake dynamometer was a digital spring scale shown in Figure 29. The load capacity of the scale is 40 kg, and is accurate to  $\pm 10$  grams.



Figure 29: Portable Electronic Spring Scale

The angular velocity of the turbine was also measured during experimental testing. Angular velocity was measured in units of revolutions per minute (rpm) using a digital laser tachometer, shown in Figure 30. The operational range of this instrument is 2.5 to 99,999 rpm and is accurate to  $\pm 0.05\%$ .



Figure 30: Digital Laser Tachometer

The hand-held digital anemometer, shown in Figure 31, measured the wind speed at the turbines face. This model was capable of measuring wind speeds up to 30 m/s, at an accuracy of  $\pm 0.1$  m/s.



Figure 31: Digital Anemometer



## Results

The results are reported following the two distinct questions investigated by the Methodology, Enclosure Verification and Directional Control.

### Enclosure Verification

The enclosure was tested at two wind speeds, the low (2 m/s) and high (3.7 m/s) settings on the fan governor. The fastest recorded angular velocity of the turbine with no load was used to calculate the VAWT's tip-speed ratio of 1.1. This result is close to the suggested optimal tip-speed ratio for a VAWT of 0.8, as defined by research included in the Literary Review.

The collected data is shown in measurements of the coefficient of performance and power curves in relation to the turbines angular velocity. Figures 32 - 35 contain two series of data. Blue data points represent tests without the enclosure, and red data points represent a tests with the enclosure attached.

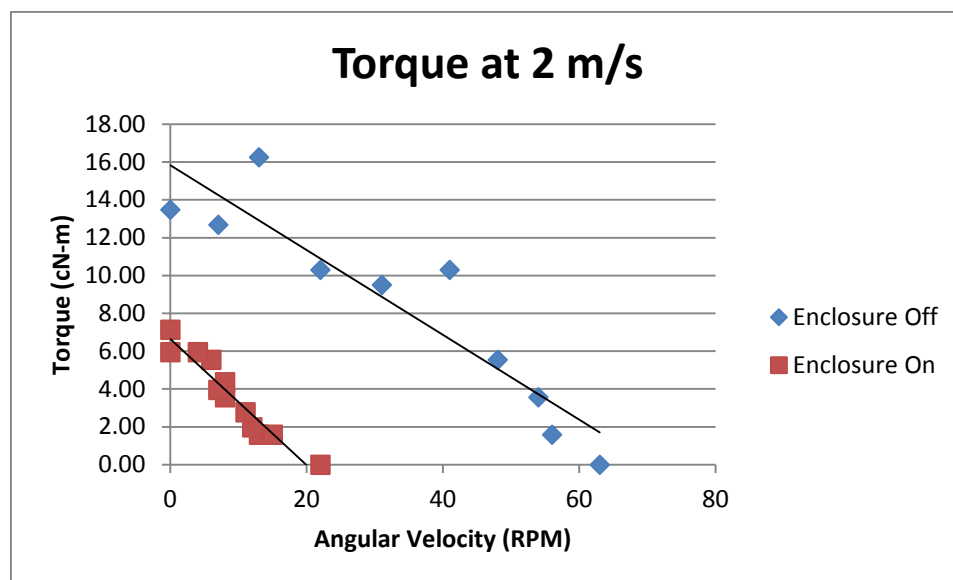


Figure 32: Torque at Low Wind Speed

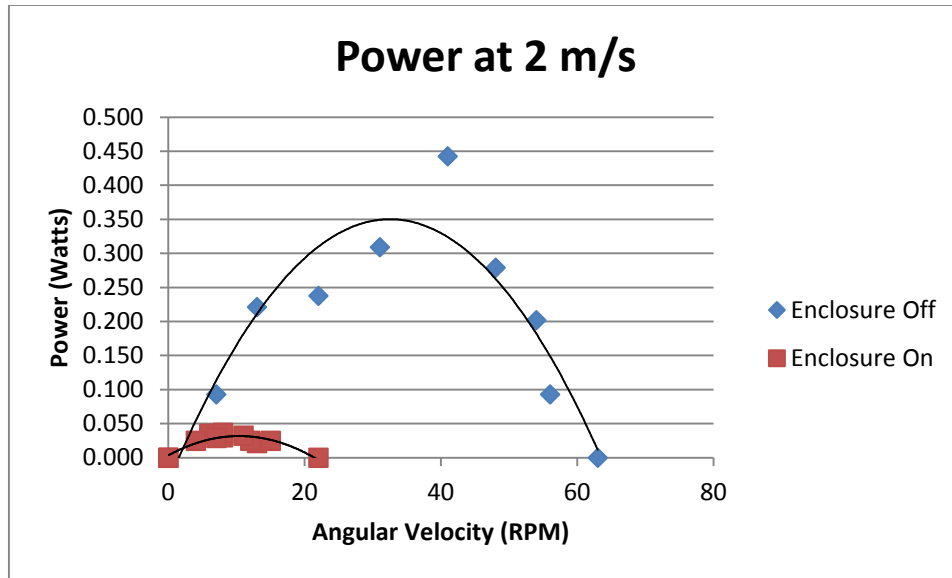


Figure 33: Power at Low Wind Speed

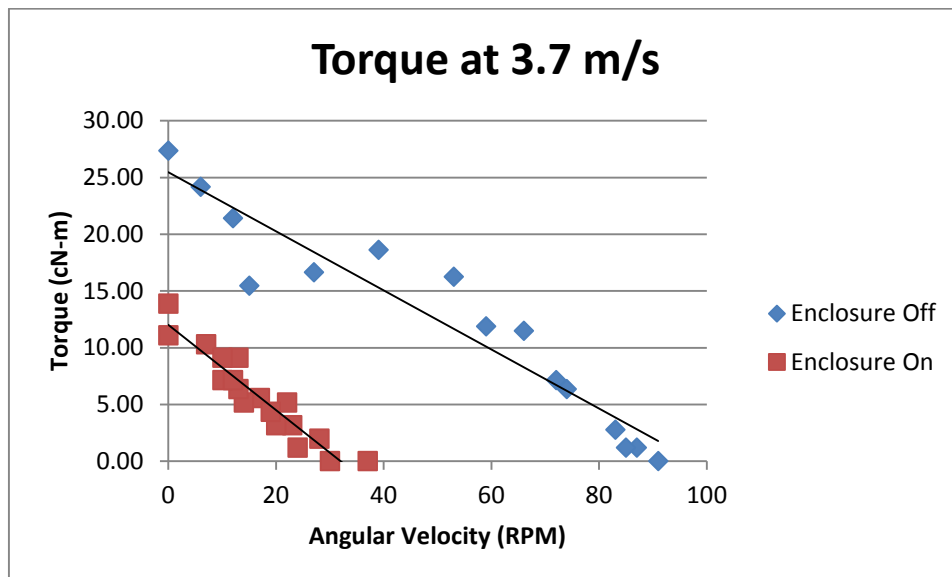


Figure 34: Torque at High Wind Speed

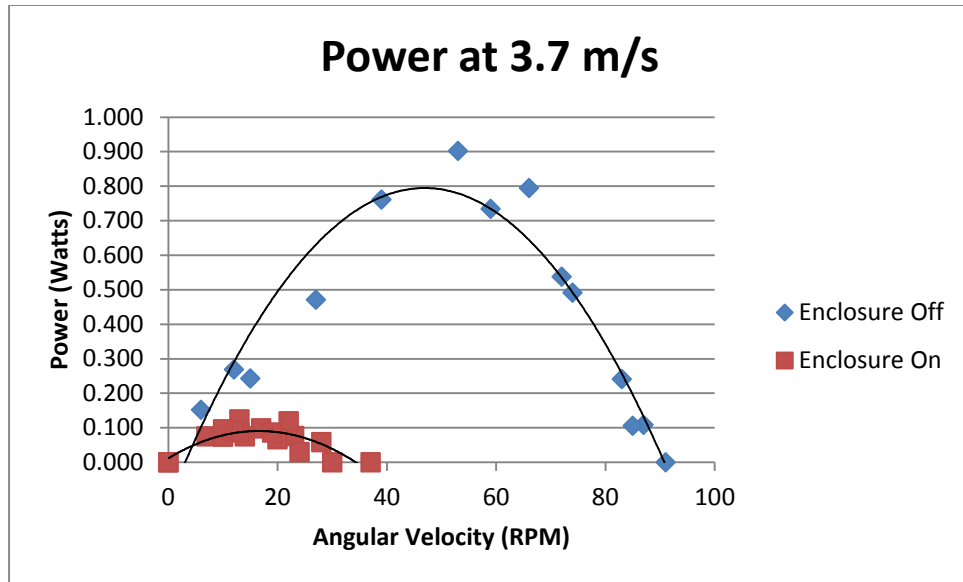


Figure 35: Power at High Wind Speed

As is demonstrated in all four figures, the turbine performed unfavorably with the partial enclosure attached. At the higher wind speed, the coefficient of performance of the turbine without the enclosure was 0.054, and with the enclosure, it decreased to 0.015. At lower wind speed, the coefficient of performance decreased from 0.168 to 0.028 when the enclosure was attached. Table 7 below further summarizes other calculated results.

Table 7: Summary of Enclosure Validation Tests

Observed Property	Percent Change
Torque, low wind	-56%
Torque, high wind	-86%
Power, low wind	-49%
Power, high wind	-92%
Coefficient of Performance, low wind	-83%
Coefficient of Performance, high wind	-72%

As demonstrated in Table 7, the effect of the enclosure on the performance of the turbine has been negative under all conditions. A discussion of why these results may disagree with the results from Brandmeier, et al. can be seen in the Discussion section.

## Direction Control

The directional control was quantitatively evaluated by timing the reaction of the tail vane to different wind directions. It was also evaluated by observation. Figure 36 shows the amount of time that elapsed as the tail vane aligned the enclosure system to the correct orientation from various starting positions. Each offset position test consisted of two trials.

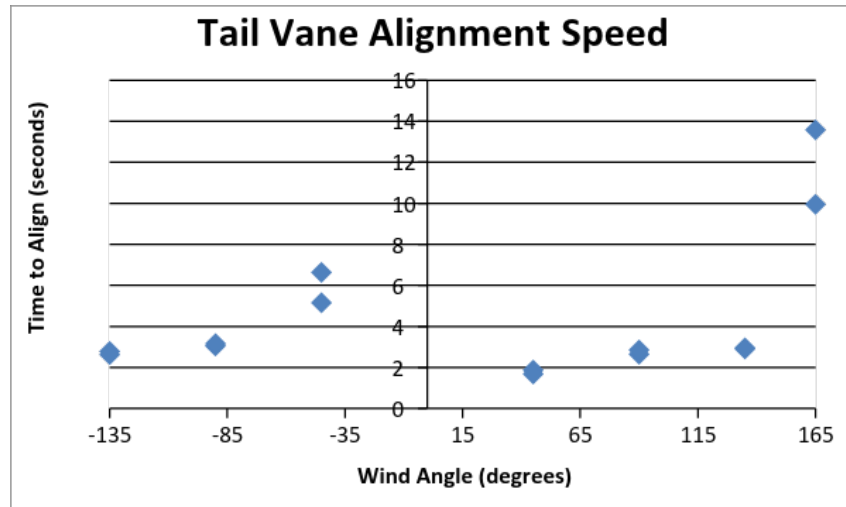


Figure 36: Tail Vane Alignment Reaction Speed

As demonstrated in the data, the direction of wind change has a notable effect on the reaction time of the tail vane. Positive angles, wind blowing into the enclosure creating a mostly blocked front facing area, were adjusted to quicker than negative angles. Notice that with the exception of the tail vane being aligned directly into the wind, the -45 degree data points took longer than any other wind angle to align the enclosure. At 180 degrees, the enclosure rotated around the positive direction, fully blocking the turbine from oncoming wind during the alignment.

Observational assessment of the tail vane allowed assessment of the performance of the tail vane in ways that are not captured by the reaction time test. Under steady conditions, the tail vane maintains a straight alignment with little oscillation, which is critical to the success of the turbine in the environment. There was some concern that the tail vane would find equilibrium on a skewed angle; that did not occur. If that were the case, the position or mounting angle of the tail vane would have to be adjusted. When the wind angle changes, there is a few second lag before the enclosure is realigned with the wind.

## Discussion

### Enclosure Verification

After comparing the results of the enclosure evaluation, it was determined that the partial enclosure reduced the coefficient of performance significantly by 83% in low wind speed and 72% in high wind speed tests. The other two calculated characteristics, output torque and power, also demonstrated large decreases in both wind conditions. These results clearly contradict the conclusions determined by Brandmaier, et al. There are two primary factors that may have led to the conflicting results, as well as other notable challenges that may have affected the results. These factors include the difference in blade shape and variations in enclosure dimensions, as well as testing setup challenges.

The most significant difference between the two studies is the blade shape. Brandmaier, et al., designed a turbine with flat blades during their testing, as opposed to the Savonius blades chosen due to their increased coefficient of performance and ability to self-start, both critical for small scale VAWTs. The difference in blade shape has significant effects on the fluid flow primarily due to turbine solidity and appears to have great effect on the merits of an enclosure. The tested enclosure shape had been optimized for flat blade turbines, so by extension there may be a shape more optimal for Savonius blades, which have much higher solidity than flat blades, which relies on an entirely different flow strategy to increase performance.

The second factor that may contribute to contrasting results is that a dimension regarding the distance between the turbine and enclosure was omitted from the prototype drawings in the study conducted by Brandmaier, et al. This space will affect the fluid flow inside the turbine blades and enclosure and affect its coefficient of performance. As a result, an approximation was made following a significant scale increase in the entire turbine system, which may lead to conflicting results.

There were additional limitations that restricted testing options. Since one objective of the project was to test the prototype for “real world” application, the ideal testing environment would have been in an outdoor setting with a data acquisition system. However, initial testing of the turbine required a controlled environment. As a result, a testing procedure that relied on a floor fan was adopted, for its advantages in providing constant wind speed and directions, a necessity when recording data manually with handheld devices.

The available wind tunnels were inadequate for the scale of the studied turbine, so a large floor fan was used as a controlled wind source. The floor fan posed many limitations in regards to its airspeed uniformity, max wind speed, and diameter. The wind speed generated by the fan was nearly zero at the center and increased radially outward. It was clear that the tests were performed without uniform flow across the turbine, but it was unclear how this inconsistency may have affected the fluid flow. The output area of the fan was a different shape than the turbine swept area, which created further inconsistencies in creating uniform flow. Given the variability in wind speeds, an approximation of the average wind speed over the turbine had to be used. Since fan output was limited, the maximum observable wind speed was lower than projected real-world conditions, causing the turbine to produce a lower torque than design estimates. The torque produced was not enough to overcome the startup torque of the motor. As a result, the use of a brake dynamometer was used to measure torque, which provided more reliable results. These factors made the testing scenario vary considerably from real-world, outdoor performance.

## Direction Control

The tail vane was able to effectively rotate the enclosure into the optimal position from various initial positions. Predictably, the slowest time occurred when the tail vane was in the 180° position, as it took some time before the tail vane was far enough to one side to catch the wind. In outdoor scenarios

this would not be a concern as the wind is seldom perfectly straight long enough for this delay to occur. Aside from this position, the  $-45^\circ$  position was the next slowest. This result was also expected because in this position the enclosure and tail vane are on opposite sides of the turbine in respect to the wind source. The enclosure catches wind and enacts a torque on the shaft just like the tail vane, and in this  $-45^\circ$  position they are opposed. Since the enclosure caused a decrease in coefficient of performance, the usefulness of the tail vane is questionable. Any redesign of the enclosure will require revising the design strategy of the tail vane.



## Recommendations

### Enclosure Verification

After it was determined that the enclosure reduced the coefficient of performance, some ad hoc experimentation led to a new conceptual path for an enclosure for Savonius blades. Barriers were arranged as depicted in Figure 37 to generate a funneling effect towards the advancing blade, increasing the speed of the incoming wind. These barriers concentrated the wind on the advancing blade, and led to a power increase of 34%. This test was only conducted with the fan speed governor set to high (3.7 m/s).

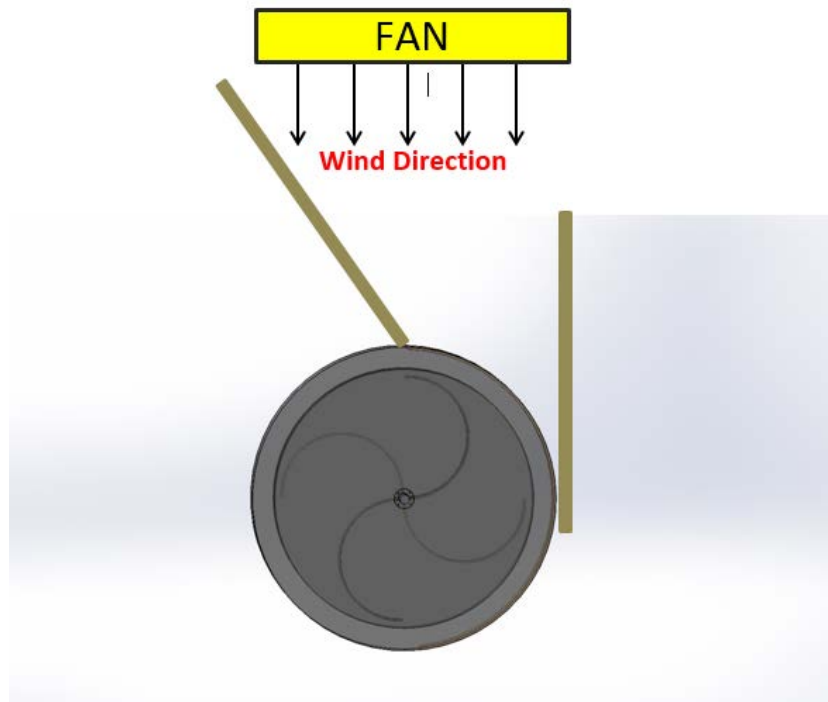


Figure 37: Funneling Experimental Setup

It was concluded that the funneling of the wind increased power more effectively than blocking

the wind from hitting the returning blade. Figure 38 and 39 below overlay the torque results of the wind funneling set up with the previously recorded data with the enclosure on and off.

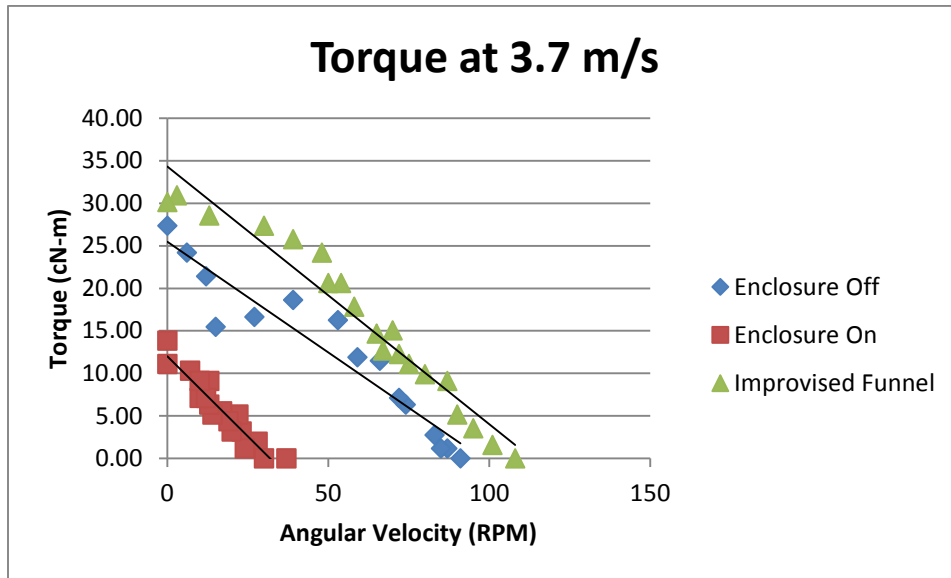


Figure 38: Torque Comparison of Funneling Setup

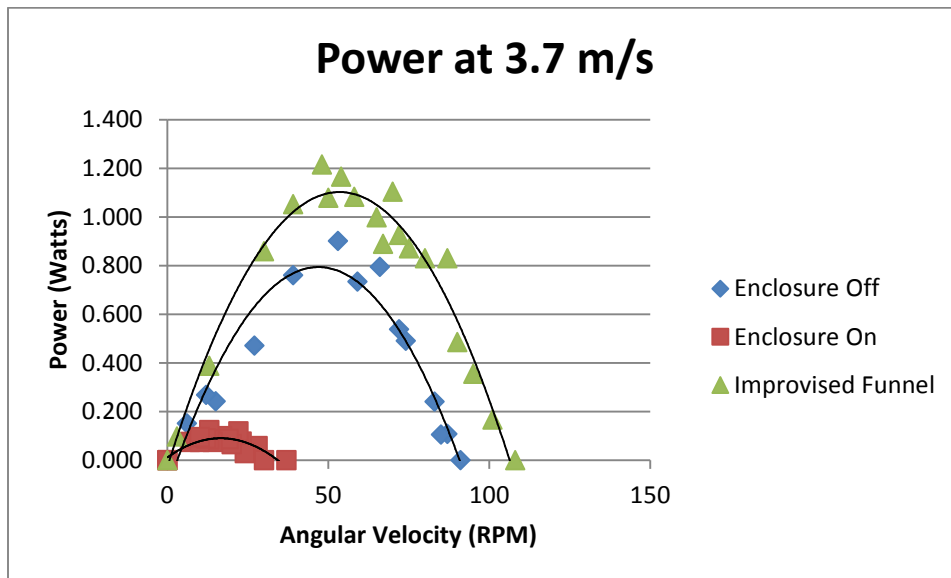


Figure 39: Power Comparison of Funneling Setup

A similar setup where the front barrier was placed blocking the same area of the turbine without funneling it into the blades performed much worse. Future efforts to design an enclosure for Savonius bladed VAWTs could focus on an enclosure that operates principally as a funnel or Venturi seem to be much more fruitful than an enclosure that blocks wind from the returning blades, the desired effect of the partial enclosure proposed by Brandmaier, et al.

## **Directional Control**

A wind concentrating enclosure would also need to be aligned with wind direction. The shape and size of the new enclosure design will determine whether a passive or active alignment device should be used. If the enclosure increases in profile by any substantial margin, an active device may be needed.

## Conclusion

VAWT technology is a promising energy harnessing vessel for low speed and multidirectional wind environments. As with all technologies, research and development can discover improvements in coefficient of performance of VAWTs. Brandmaier, et al. presented research that a partial enclosure across half the front-facing swept area of a flat bladed turbine improved the angular velocity of the turbine, suggesting an increase in the coefficient of performance. The goal of this project was to design, build, and evaluate a Savonius VAWT prototype with the Brandmaier, et al, enclosure and a wind alignment device.

Through experimental testing, the Brandmaier, et al, enclosure was found to reduce the torque output, power output, and the coefficient of performance of the VAWT in both low and high wind speed configurations. Results from brake dynamometer measurements of the turbine with the partial enclosure attached exhibited decreases in coefficient of performance by 92% and 86%, torque output by 56% and 86%, and power output by 49% and 92%, for low and high wind speed, respectively. However, ad hoc testing of the funneling arrangement improved the coefficient of performance 34% against the results of those without the enclosure.

A passive tail vane was proposed to enable the enclosure to continuously reorient itself in the optimal position contingent on the wind direction. After testing the tail vane in seven offset positions at multiples of  $45^\circ$ , it was concluded the tail vane acts properly, and rotates the enclosure to the correct orientation regardless of the wind direction including completely opposing wind. Although the overall results prove the effectiveness of the current tail vane and enclosure system, any modification to the enclosure design will mandate a reevaluation of an appropriate wind alignment device.

## Bibliography

- Berg, D. (1990). Customized Airfoils and their Impact on VAWT Cost of Energy. Albuquerque, NM: Sandia National Laboratories.
- Brain, M. (2000). How Horsepower Works. Retrieved 5 Sept 2013, 2013, from <http://auto.howstuffworks.com/horsepower.htm>
- Brandmaier, C., Everett, J., Hassan, A., Kates, A.,. (2013). *Enclosed Wind Turbines*. Worcester, MA U6 - ctx\_ver=Z39.88-2004&ctx\_enc=info%3Aofi%2Fenc%3AUTF-8&rft\_id=info:sid/summon.serialssolutions.com&rft\_val\_fmt=info:ofi/fmt:kev:mtx:book&rft.genre=book&rft.title=Enclosed+Wind+Turbines&rft.au=Kates%2C+Andrea+Erin+Student+author+--+ME&rft.au=Hassan%2C+Anthony+Joseph+Student+author+--+ME&rft.au=Everett%2C+James+Nichols+Student+author+--+ME&rft.au=Brandmaier%2C+Christopher+G.+Student+author+--+ME&rft.date=2013-01-01&rft.pub=Worcester+Polytechnic+Institute&rft.externalDocID=1849504&paramdict=en-US U7 - eBook U8 - FETCH-wpi\_catalog\_18495041: Worcester Polytechnic Institute.
- Bravo, R., Tullis, S., & Ziada, S. (n.d.). Performance Testing of a Small Vertical-Axis Wind Turbine. [http://www.eng.mcmaster.ca/~stullis/index\\_files/Bravo%20CANCAM%202007.pdf](http://www.eng.mcmaster.ca/~stullis/index_files/Bravo%20CANCAM%202007.pdf)
- Chatterjee, P., & Laoulache, R. N. Performance Modeling of Ducted Vertical Axis Turbine Using Computational Fluid Dynamics. 47(July/August 2013).
- Chih-Hsien, W., & Tsai, Y.-F. (<sup>2011</sup>). United States Patent No.
- Chinchilla, R., Guccione, S., & Tillman, J. (2011). Wind Power Technologies: A Need for Research and Development in Improving VAWT's Airfoil Characteristics. *Journal of Industrial Technology*, 27(1).
- Elliot, R. (2001). Beginners' Guide to Potentiometers: **Elliott Sound Products**.
- Enevoldsen, P. B., Frydendal, I., Poulsen, S., & Rubak, R. (2010). US 2010/0102559. S. Corporation.
- Eriksson, S., Bernhoff, H., & Leijon, M. (2008). Evaluation of different turbine concepts for wind power. 12, 1419-1434.
- Fiberglass: A Cost Effective Solution To Sheet Metal. (2013). from <http://www.performancecomposites.com/downloads.html>
- Gipe, P. (1995). *Wind Energy Comes of Age*. Canada: John Wiley & Sons.

- Golecha, K., Eldho, T. I., & Pradbu, S. V. Performance Study of modified Savonius water turbine with two deflector plates. Bombay, India: Indian Institute of Technology.
- Greenpeace. (2013). Quit Coal. Retrieved September 29th, 2013, from <http://www.greenpeace.org/international/en/campaigns/climate-change/coal/>
- Guittet, L., Kusulja, M., & Maitre, T. (2004). Setting up of an experiment to test vertical axis water turbines.
- Heath, M. A., Walshe, J. D., & Watson, S. J. (2007). Estimating the potential Yield of Small Building-mounted Wind Turbines. *Wind Energy*, (10), 271-287.
- Holak, R., & Mourkas, M. (2012). Enclosed Vertical Axis Wind Turbines (pp. 41): Worcester Polytechnic Institute.
- Islam, M. (2010). *Design and Development of a Vertical Axis Micro Wind Turbine*. (Master of Science), University of Manchester.
- Islam, M., Ahmed, F. U., Ting, D. S., & Fartaj, A. (2008). Design analysis of fixed-pitch straight-bladed vertical axis wind turbines with an alternative material. *Retrieved May, 5, 2010*.
- Islam, M., Ting, D. S.-K., & Fartaj, A. (2008). Aerodynamic models for Darrieus-type straight-bladed vertical axis wind turbines. *Renewable and Sustainable Energy Reviews*, 12(4), 1087-1109.
- Islam, M. Q., Hasan, M. N., & Saha, S. (2005). *EXPERIMENTAL INVESTIGATION OF AERODYNAMIC CHARACTERISTICS OF TWO, THREE AND FOUR BLADED S-SHAPED STATIONARY SAVONIUS ROTORS*. Paper presented at the The Proceeding of International Conference on Mechanical Engineering.
- Johnson, G. L. (1985). *Wind energy systems*: Prentice-Hall Englewood Cliffs (NJ).
- Kodric, A. A. (1989). United States Patent No.
- Kroldrup, L. (2010). Gains in Global Wind Capacity Reported, *The New York Times*. Retrieved from <http://green.blogs.nytimes.com/2010/02/15/gains-in-global-wind-capacity-reported/>
- Kuo, Hai P. (2011) U.S Patent “Wind turbine with gale protection”: Google Patents
- Letcher, T. (2010). Small Scale Wind Turbines Optimized for Low Wind Speeds.
- Manwell, J. F., McGowan, J. G., & Rogers, A. L. (2002). *Wind Energy Explained - Theory, Design & Applications* (1 ed.): Wiley.
- Menet, J., Valdes, L., & Menart, B. (2001). A Comparative Calculation of the Wind Turbines

Capacities on the Basis of the  $L$ - $\sigma$  Criterion (pp. 491-506).

Mohamed, M. H., Janiga, G., Pap, E., & Thévenin, D. (2010). Optimization of Savonius turbines using an obstacle shielding the returning blade. *Renewable Energy*, 35(11), 2618-2626. doi: <http://dx.doi.org/10.1016/j.renene.2010.04.007>

Mohamed, M. H., Janiga, G., Pap, E., & Thévenin, D. (2011). Optimal blade shape of a modified Savonius turbine using an obstacle shielding the returning blade. *Energy Conversion and Management*, 52(1), 236-242. doi: <http://dx.doi.org/10.1016/j.enconman.2010.06.070>

Paraschivoiu, I. (2002). *Wind Turbine Design: With Emphasis on Darrieus Concept*

Peinke, J., Schaumann, P., & Barth, S. (2007). *Wind Energy: Proceeding of the Euromech Colloquium*: Springer-Verlang Berlin Heidelberg.

Poole, A. B. (2007). Infuser augmented vertical wind turbine electrical generating system: Google Patents.

Saha, U., Thotla, S., & Maity, D. (2008). Optimum design configuration of Savonius rotor through wind tunnel experiments. *Journal of Wind Engineering and Industrial Aerodynamics*, 96(8), 1359-1375.

Seguro, J., & Lambert, T. (2000). Modern estimation of the parameters of the Weibull wind speed distribution for wind energy analysis. *Journal of Wind Engineering and Industrial Aerodynamics*, 85(1), 75-84.

WindStreamPower. (2013). Permanent Magnet DC Generator 443540. Retrieved 9/12/2013

Wortman, A. J. (1983). *Introduction to Wind Turbine Engineering*: Butterworth-Heinemann.

# Appendices

## Appendix A: Design Proof Calculations

These calculations are shown with preliminary values that have been altered numerous times throughout the design and experimental testing processes. However, the governing equations have remained intact.

### Turbine sizing, Power output, and Cut-in Speed

Turbine Dimensions:

$$h := 3\text{ft}$$

$$\alpha := 1.5$$

$$D := \frac{h}{\alpha} = 2\text{-ft}$$

$$r := \frac{D}{2} = 1\text{-ft}$$

$$A := h \cdot r = 0.279\text{m}^2$$

Wind Characteristics:

$$V_{\text{mean}} := 10 \frac{\text{m}}{\text{s}}$$

$$V_{\text{mean}} = 22.369\text{-mph}$$

$$\rho := 1.1839 \frac{\text{kg}}{\text{m}^3}$$

Operational Parameters:

$$t_{\text{sr}} := .8$$

$$c_p := 0.29$$

coefficient of performance is a function of tip speed ratio. This value is a guess.

$$\omega := \frac{V_{\text{mean}}}{t_{\text{sr}} \cdot r} = 391.621\text{-rpm}$$

Output Ratings:

$$P := 0.5 \cdot \rho \cdot V_{\text{mean}}^3 \cdot A \cdot c_p = 47.845\text{ W} \quad P = 0.064\text{-hp}$$

$$T := \frac{P}{\omega} = 1.167\text{-N}\cdot\text{m}$$

$$T = 0.86\text{-lbf}\cdot\text{ft}$$

Startup Torque and Cut-in Speed:

$$T_{\text{gen}} := .043\text{-lbf}\cdot\text{ft}$$

$$\gamma := 0.8$$

gamma is the mechanical losses incurred in the system before the generator

$$T_{\text{cutin}} := \frac{T_{\text{gen}}}{\gamma} = 0.645\text{-lbf}\cdot\text{in}$$

$$c := \frac{r}{2} = 0.152\text{m}$$

$$F_{\text{needed}} := \frac{T_{\text{cutin}}}{c} = 0.478\text{ N}$$

Note: torque calculation was simplified as a distributed force on a cantilevered flat-planar surface, rather than a surface with curvature.

$$P_{\text{wind}} := \frac{F_{\text{needed}}}{A} = 1.716\text{ Pa}$$

$$V_{\text{cutin}} := \sqrt{\frac{P_{\text{wind}}}{\rho}} = 1.204 \frac{\text{m}}{\text{s}} \quad V_{\text{cutin}} = 2.693\text{-mph}$$



## Shaft Stresses due to Generated Torque and System Weight

(Torque applied throughout the shaft, weight as a point force on top of the shaft)

Sizing the turbine shaft based on applied torque and weight of turbine and enclosure

$$L_{ft} := 3.5$$

$$L_{mm} := 1.067 \text{ m} \quad D_1 := .013 \quad \text{m} \quad A_1 := \frac{\pi}{4} \cdot D_1^2 = 1.327 \times 10^{-4} \quad \text{m}^2 \quad D := .5 \cdot \text{in}$$

$$c_A := \frac{D_1}{2} = 6.5 \times 10^{-3} \quad \text{m} \quad D = 0.013 \text{ m}$$

$$I := \frac{\pi}{4} \cdot \left( \frac{D_1}{2} \right)^4 = 1.402 \times 10^{-9} \quad \text{m}^4$$

The critical section is at the motor, which acts as a wall in the cantilever calculation model.

weight of the enclosure and turbine

$$w := 100 \quad \text{Newtons}$$

$$w_{\text{newtons}} := 100 \text{ N}$$

$$w_{\text{newtons}} = 22.481 \cdot \text{lbf}$$

$$\sigma_x := \frac{w}{A_1} = 7.534 \times 10^5$$

torque from shaft rotation:

$$P_{\text{gen}} := 100 \quad \text{W}$$

$$w_{\text{rpm}} := 200 \quad \text{rpm}$$

$$\omega := w_{\text{rpm}} \cdot \frac{2\pi}{60} = 20.944$$

$$T_{\text{gen}} := \frac{P_{\text{gen}}}{\omega} = 4.775 \quad \text{Nm}$$

$$\tau_{xzA} := \frac{T \cdot \left( \frac{D_1}{2} \right)}{2 \cdot I} = 1.107 \times 10^7$$

Principle Stresses at A

$$\sigma_{xA} := \sigma_x \quad \sigma_{yA} := 0 \quad \sigma_{zA} := 0$$

$$\tau_{xy} := 0 \quad \tau_{xz} := \tau_{xzA} \quad \tau_{yz} := 0$$

$$C_2 := \sigma_{xA} + \sigma_{yA} + \sigma_{zA} = 7.534 \times 10^5$$


---

## Principle Stresses at A

$$\sigma_{xA} := \sigma_x \quad \sigma_{yA} := 0 \quad \sigma_{zA} := 0$$

$$\tau_{xy} := 0 \quad \tau_{xz} := \tau_{xzA} \quad \tau_{yz} := 0$$

$$C_2 := \sigma_{xA} + \sigma_{yA} + \sigma_{zA} = 7.534 \times 10^5$$

$$C_1 := \tau_{xy}^2 + \tau_{xz}^2 + \tau_{yz}^2 - \sigma_{xA} \cdot \sigma_{yA} - \sigma_{xA} \cdot \sigma_{zA} - \sigma_{yA} \cdot \sigma_{zA} = 1.225 \times 10^{14}$$

$$C_0 := \sigma_{zA} \cdot \sigma_{yA} \cdot \sigma_{zA} + 2 \cdot \tau_{xy} \cdot \tau_{xz} \cdot \tau_{yz} - \sigma_{xA} \cdot \tau_{yz}^2 - \sigma_{yA} \cdot \tau_{xz}^2 - \sigma_{zA} \cdot \tau_{xy}^2 = 0$$

$$f(\sigma) := \sigma^3 - C_2 \cdot \sigma^2 - C_1 \cdot \sigma - C_0$$

$$C_{\text{ww}} := f(\sigma) \text{ coeffs}, \sigma \rightarrow \begin{pmatrix} 0 \\ -1.2250755682891491e14 \\ -753396.18031666428 \\ 1 \end{pmatrix}$$

$$r := \text{polyroots}(C) = \begin{pmatrix} -1.07 \times 10^7 \\ 0 \\ 1.145 \times 10^7 \end{pmatrix}$$

The roots are sigma1,2,3, in order sigma1 as the greatest to sigma3 as the least

$$\sigma_{1A} := r_2 = 1.145 \times 10^7 \quad \sigma_{2A} := r_1 = 0 \quad \sigma_{3A} := r_0 = -1.07 \times 10^7$$

$$\tau_{\max A} := \frac{(\sigma_{1A} - \sigma_{3A})}{2} = 1.107 \times 10^7$$

$$\sigma_{vMA} := \sqrt{\sigma_{1A}^2 + \sigma_{2A}^2 + \sigma_{3A}^2 - \sigma_{1A} \cdot \sigma_{2A} - \sigma_{1A} \cdot \sigma_{3A} - \sigma_{2A} \cdot \sigma_{3A}} = 1.919 \times 10^7$$

Material: 5052 Aluminum, cold rolled

$$S_y := 255 \cdot 10^6$$

$$N_{\text{dist}A} := \frac{S_y}{\sigma_{vMA}} = 13.291$$

Ndist is the distortion energy theory

$$N_{\text{shear}A} := \frac{0.5 S_y}{\tau_{\max A}} = 11.513$$

Nshear is the maximum shear stress theory

The distortion energy theory gives a much less conservative safety factor.

Endurance Limit and corection factors

For  $10^6$  cycles, find  $S_e$

$$S_{ut} := 300 \text{ MPa}$$

$$S_{e1} := \begin{cases} \text{return } 0.5 \cdot S_{ut} & \text{if } S_{ut} \leq 200 \\ 100 & \text{otherwise} \end{cases}$$

$$S_{e1} = 100$$

$$C_{load} := .58 \quad \text{for torsion}$$

$$C_{size} := 0.85$$

$$A_s := 4.51 \quad b_s := -.265$$

$$C_{surf} := A_s \cdot (S_{ut})^{b_s} = 0.995$$

$$C_{temp} := 1$$

$$C_{reliab} := .702$$

$$S_e := C_{load} \cdot C_{size} \cdot C_{surf} \cdot C_{temp} \cdot C_{reliab} \cdot S_{e1} = 34.429 \text{ MPa}$$

at  $10^6$  cycles

Graph the High Cycle Fatigue Region

$$L_{loading} := \text{"axial"}$$

$$S_m := \begin{cases} (.9 \cdot S_{ut}) & \text{if } L_{loading} = \text{"bending"} \\ (.75 \cdot S_{ut}) & \text{if } L_{loading} = \text{"axial"} \end{cases}$$

$$S_m = 225$$

$$b := \frac{-1}{3} \cdot \log\left(\frac{S_m}{S_e}\right) = -0.272$$

Graph the High Cycle Fatigue Region

$$L_{\text{loading}} := \text{"axial"}$$

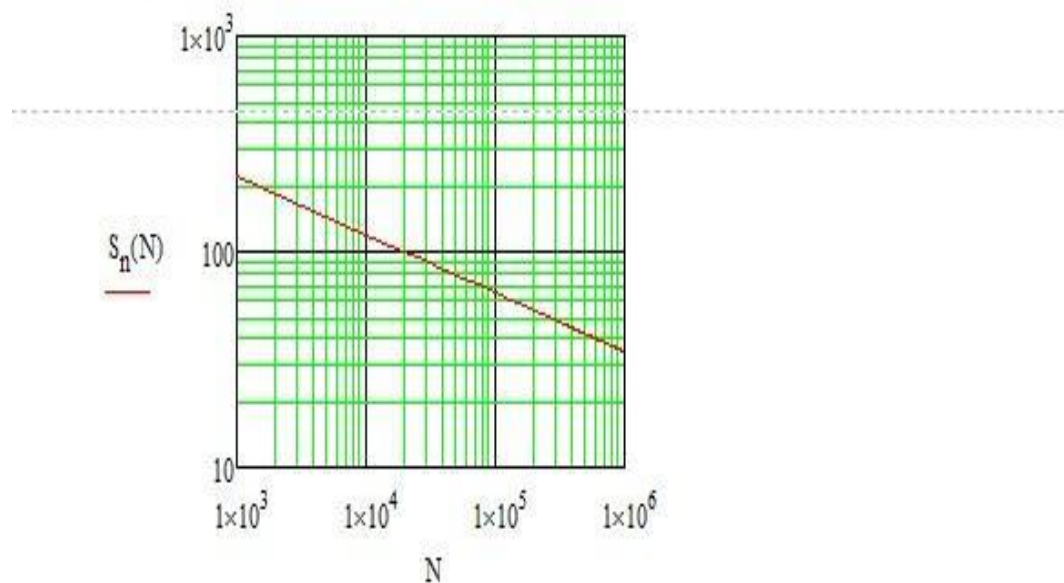
$$S_m := \begin{cases} (.9 \cdot S_{ut}) & \text{if } L_{\text{loading}} = \text{"bending"} \\ (.75 \cdot S_{ut}) & \text{if } L_{\text{loading}} = \text{"axial"} \end{cases}$$

$$S_m = 225$$

$$b := \frac{-1}{3} \cdot \log\left(\frac{S_m}{S_e}\right) = -0.272$$

$$a := \frac{S_e}{10^{6 \cdot b}} = 1.47 \times 10^3$$

$$S_n(N) := a \cdot N^b \quad N := 10^3, 10^4 \dots 10^6$$



$$S_n(10^3) = 225$$

$$S_n(10^6) = 34.429$$

## Shaft Deflection due to Wind Load

(Linear distributed wind load on a spherical object the diameter of the enclosure,  
and the moment induced by the weight of the tail vane.  
Structural support provided only by the shaft)

Given Values:

$$od := 2\text{ft} \quad d_{\text{shaft}} := 1\text{in}$$

od is the diameter of the area affected by wind.  
dshaft is the diameter of the shaft, which is  
providing all the support

$$l := 3\text{ft}$$

$$I := \frac{\pi}{64} \cdot (d_{\text{shaft}}^4) = 2.043 \times 10^{-8} \cdot \text{m}^4$$

$$E := 70\text{GPa}$$

$$v := 30\text{mph}$$

Wind Speed

$$\rho := 1.25 \frac{\text{kg}}{\text{m}^3}$$

Air Density

$$A := 1 \cdot od = 6 \cdot \text{ft}^2$$

Area of tower effected by wind

$$c_p := 1$$

Drag coefficient

$$P := \frac{1}{2} \cdot \rho \cdot c_p \cdot v^2 = 0.016 \cdot \text{psi}$$

Pressure due to wind

$$F := P \cdot A = 14.087 \cdot \text{lbf}$$

Force of wind on tower

$$w := \frac{F}{l} = 4.696 \cdot \frac{\text{lbf}}{\text{ft}}$$

$$M_{\text{vane}} := 1 \text{ lbf} \cdot \text{in}$$

Singularity Functions:

$$q(x) = -M_1 \langle x - 0 \rangle^{-2} - M_{\text{vane}} \langle x - 0 \rangle^{-2} + R_1 \langle x - 0 \rangle^{-1} - w \langle x - l \rangle^0$$

$$V(x) = -M_1 \langle x - 0 \rangle^{-1} - M_{\text{vane}} \langle x - 0 \rangle^{-1} + R_1 \langle x - 0 \rangle^0 - w \langle x - l \rangle^1 + C_1$$

$$M(x) = -M_1 \langle x - 0 \rangle^0 - M_{\text{vane}} \langle x - 0 \rangle^0 + R_1 \langle x - 0 \rangle^1 - w/2 \langle x - l \rangle^2 + C_1 x + C_2$$

$$\theta(x) = (-M_1 \langle x - 0 \rangle^1 - M_{\text{vane}} \langle x - 0 \rangle^1 + R_1 \langle x - 0 \rangle^2/2 - w \langle x - l \rangle^3/6 + C_1 x^2/2 + C_2 x + C_3) / EI$$

$$y(x) = (-M_1 \langle x - 0 \rangle^2/2 - M_{\text{vane}}/2 \langle x - 0 \rangle^2 + R_1 \langle x - 0 \rangle^3/6 - w \langle x - l \rangle^4/24 + C_1 x^3/6 + C_2 x^2/2 + C_3 x + C_4) / EI$$

$$C_2 := 0 \quad C_1 := C_2 = 0$$

Look at boundary conditions when  $x=l$ ,  $V=0$  and  $M=0$

$$V = R_1 - w \cdot l = 0$$

$$R_1 := w \cdot l = 0.063 \cdot \text{kN}$$

$$M = -M_1 + R_1 \cdot l - \frac{w}{2} \cdot (l - l)^2 = 0$$

$$M_1 := R_1 \cdot l - \frac{w}{2} \cdot (l - l)^2 = 42.26 \cdot \text{lbf} \cdot \text{ft} \quad \text{clockwise}$$

Boundary conditions, when  $x=0$ ,  $\theta=0$  and  $y=0$

$$C_3 := M_1 \cdot 0^1 - R_1 \cdot 0^2 = 0$$

$$C_4 := \frac{M_1}{2} \cdot 0^2 - \frac{R_1}{6} \cdot 0^3 = 0$$

Maximum Deflection at free end:

$$y_{\max} := \frac{1}{E \cdot I} \left[ \frac{-M_1 \cdot l^2}{2} + \frac{R_1}{6} \cdot (l)^3 - \frac{M_{\text{vane}}}{2} \cdot (l)^2 - \frac{w}{24} \cdot (l-l)^4 \right] = -0.441 \cdot \text{in}$$

Graph the Diagrams

Range of  $x$                        $x := 0 \cdot \text{in}, 0.005 \cdot l \dots l$

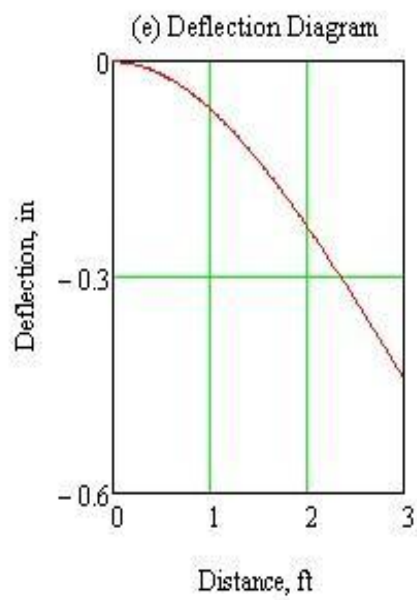
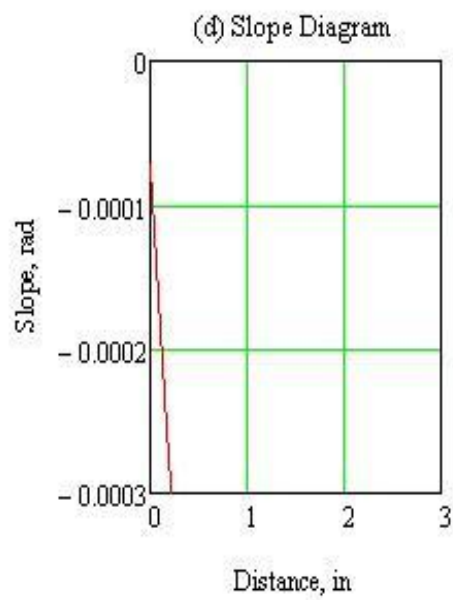
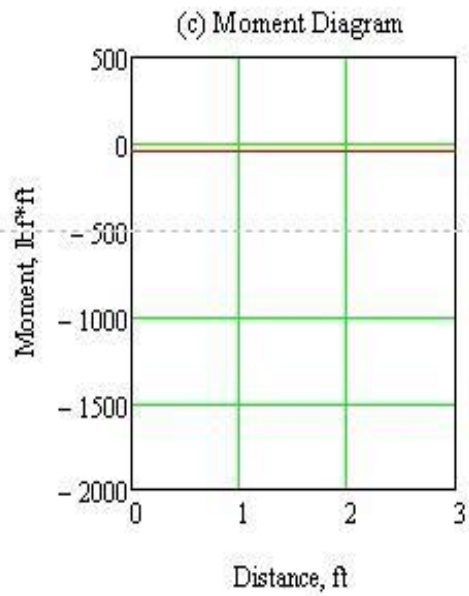
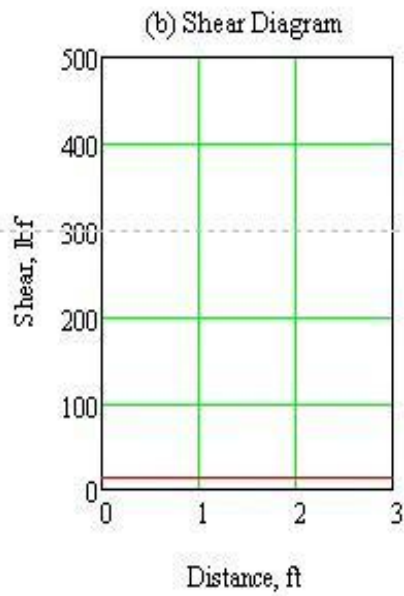
Unit step function               $S(x, z) := \text{if}(x \geq z, 1, 0)$

$$V(x) := R_1 \cdot S(x, 0 \cdot \text{in}) \cdot (x - 0)^0 - w \cdot S(x, l) \cdot (x - l)^1$$

$$M(x) := -M_1 \cdot S(x, 0 \cdot \text{in}) \cdot (x - 0)^0 - M_{\text{vane}} + R_1 \cdot S(x, 0 \cdot \text{in}) \cdot (x - 0)^1 - \frac{w}{2} \cdot S(x, l) \cdot (x - l)^2$$

$$\theta(x) := \frac{1}{E \cdot I} \left[ -M_1 \cdot S(x, 0 \cdot \text{in}) \cdot (x - 0)^1 - M_{\text{vane}} \cdot (l) + \frac{R_1}{2} \cdot S(x, 0 \cdot \text{in}) \cdot (x - 0)^2 \dots \right. \\ \left. + - \left[ \frac{w}{6} \cdot S(x, l) \cdot (x - l)^3 \right] + C_3 \right]$$

$$y(x) := \frac{1}{E \cdot I} \left[ -\frac{M_1}{2} \cdot S(x, 0 \cdot \text{in}) \cdot (x - 0)^2 - \frac{M_{\text{vane}}}{2} \cdot (l)^2 + \frac{R_1}{6} \cdot S(x, 0 \cdot \text{in}) \cdot (x - 0)^3 \dots \right. \\ \left. + - \left[ \frac{w}{24} \cdot S(x, l) \cdot (x - l)^4 \right] + C_3 \cdot x + C_4 \right]$$





## Blade failure due to wind force

(modeled as a thin-walled pressure vessel)

$$r := .5\text{ft}$$

$$t := .0625\text{in}$$

$$S_y := 2\text{ksi}$$

cardboard has a yield strength of approximately 2-5ksi.  
Sonotube is wax-sealed cardboard/paper.

$$\rho := 1.25 \frac{\text{kg}}{\text{m}^3}$$

$$c_d := 2.4$$

$$V_w := 50\text{mph}$$

Find Pressure against inside of blade

$$p := 0.5 \cdot \rho \cdot c_d \cdot V^2 = 749.418 \text{ Pa}$$

Tangential and Longitudinal Stresses

$$\sigma_t := \frac{p \cdot r}{t} = 0.072 \cdot \text{MPa}$$

$$\sigma_L := \frac{p \cdot r}{2t} = 0.036 \cdot \text{MPa}$$

Principle and von Mises Stresses

$$\sigma_1 := \sigma_t$$

$$\sigma_3 := \sigma_L$$

$$\sigma_{vM} := \sqrt{\sigma_1^2 + \sigma_3^2 - \sigma_1 \cdot \sigma_3} = 0.062 \cdot \text{MPa}$$

Safety Factor

$$N := \frac{S_y}{\sigma_{vM}} = 221.321$$

## Tail Vane Stresses

### Vane Geometry

$$l_v := 12 \text{ in}$$

$$h := 6 \text{ in}$$

$$t := .5 \text{ in}$$

$$A_{yxb} := h \cdot t = 3 \cdot \text{in}^2$$

$$A_{zy} := l_v \cdot h = 72 \cdot \text{in}^2$$

$$\rho_v := 10 \frac{\text{kg}}{\text{m}^3}$$

$$V_v := l_v \cdot h \cdot t = 36 \cdot \text{in}^3$$

### Support Geometry

$$h_s := .5 \text{ in}$$

$$t_s := .5 \text{ in}$$

$$A_{yxs} := h_s \cdot t_s = 0.25 \cdot \text{in}^2$$

cross sections at base of vane at support

Area that catches wind

density of tail vane

volume of tail vane

### Wind Load

$$\rho_{\text{air}} := 1.25 \frac{\text{kg}}{\text{m}^3}$$

$$C_d := 1.98$$

$$V := 30 \text{ mph}$$

$$p := 0.5 \cdot \rho_{\text{air}} \cdot C_d \cdot V^2 = 222.577 \text{ Pa}$$

$$F_w := p \cdot A_{zy} = 10.339 \text{ N}$$

density of air

coefficient of drag of tail vane

speed of wind

pressure of wind

force of wind

Stresses due to Wind force at base  
(vane perpendicular to wind)

$$\sigma_{\text{windb}} := \frac{F_w}{A_{yxb}} = 5.342 \cdot \text{kPa}$$

stress at base

Stresses due to Wind force at base  
(vane perpendicular to wind)

$$\sigma_{windb} := \frac{F_w}{A_{yxb}} = 5.342 \cdot \text{kPa} \quad \text{stress at base}$$

$$\sigma_{winds} := \frac{F_w}{A_{yxs}} = 64.102 \cdot \text{kPa} \quad \text{stress at support}$$

Stresses due to Weight

$$F_g := V_v \cdot \rho_v \cdot 9.81 \frac{\text{m}}{\text{s}^2} = 0.058 \text{ N} \quad \text{Force due to weight}$$

$$\sigma_{gb} := \frac{F_g}{A_{yxb}} = 0.03 \cdot \text{kPa} \quad \text{stress at base}$$

$$\sigma_{gs} := \frac{F_g}{A_{yxs}} = 0.359 \cdot \text{kPa} \quad \text{stress at support}$$

Combined Stresses

$$\sigma_b := \sqrt{\sigma_{windb}^2 + \sigma_{gb}^2 - \sigma_{windb} \cdot \sigma_{gb}} = 5.327 \cdot \text{kPa} \quad \text{von Mises stress at base}$$

$$\sigma_s := \sqrt{\sigma_{winds}^2 + \sigma_{gs}^2 - \sigma_{winds} \cdot \sigma_{gs}} = 63.924 \cdot \text{kPa} \quad \text{von Mises stress at support}$$

Safety Factors

$$S_y := 5000 \text{ psi} \quad \text{yield strength of cardboard}$$

$$N_b := \frac{S_y}{\sigma_b} = 6471.565 \quad \text{safety factor at base}$$

## Safety Factors

$$S_y := 5000 \text{ psi}$$

yield strength of cardboard

$$N_b := \frac{S_y}{\sigma_b} = 6471.565$$

safety factor at base

$$N_s := \frac{S_y}{\sigma_s} = 539.297$$

safety factor at support

## Rotational time

(given constant applied torque. In reality, torque applied will decrease as the vane rotates and the perpendicular wind force component decreases to zero)

$$\theta := \frac{\pi}{2} \cdot \text{rad}$$

angle to rotate

$$D := 31.33 \text{ in}$$

Distance from centroid of force to rotational axis

$$\tau := F_w \cdot D = 8.228 \cdot \text{N} \cdot \text{m}$$

Torque applied by wind

$$I := 4418.84 \text{ lb} \cdot \text{in}^2$$

Area moment of inertia about rotational axis






$$\alpha := \frac{\tau}{I} = 6.363 \frac{1}{\text{s}^2}$$

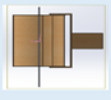

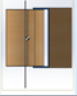


Acceleration due to torque

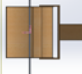




$$\theta = \theta_i + \omega \cdot t + \frac{1}{2} \cdot \alpha \cdot t^2$$

$$t := \sqrt{\frac{2\theta}{\alpha}} = 0.703 \text{ s}$$

time to rotate to  $\theta$






Tail Vane Reaction Time (s)														
Type	Area (in <sup>2</sup> )	Ixx (lb-in <sup>2</sup> )	D (in)	V = 5 mph Time (s)	V = 10 mph Time (s)	V = 15 mph Time (s)	V = 20 mph Time (s)	V = 25 mph Time (s)	V = 30 mph Time (s)	V = 35 mph Time (s)	V = 40 mph Time (s)	V = 45 mph Time (s)	W/sight (lbs)	Bending Moment for the Enclosure (lb-in)
	216	4747.77	27.26	2.705	1.352	0.902	0.676	0.541	0.451	0.386	0.338	0.301	0.62	16.9012
	1230	8668.5	33.21	1.388	0.694	0.463	0.347	0.278	0.231	0.198	0.173	0.154	3.55	117.8955
	738	5392.18	27.26	1.644	0.822	0.548	0.411	0.329	0.274	0.235	0.206	0.183	2.13	58.0638
	1250	8061.86	30.73	1.38	0.69	0.46	0.345	0.276	0.23	0.197	0.173	0.153	3.61	110.9353
	1200	7315.05	28.26	1.399	0.7	0.466	0.35	0.28	0.233	0.2	0.175	0.155	3.47	98.0622

Tail Vane Bending Stress Due To Wind (X direction)									
Type	Area (in <sup>2</sup> )	Izz (in <sup>4</sup> )	D1 (in)	b (in)	h (in)	C1 (in)	Wind Force (Lbf)	Ix (in <sup>4</sup> )	Stress X (Lbf/in <sup>2</sup> )
1 	216	4747.77	9	12	0.5	0.25			
Wind Speed = 5 mph							0.194	0.75	0.581
Wind Speed = 15 mph							1.743	0.75	5.23
Wind Speed = 25 mph							4.842	0.75	14.527
Wind Speed = 35 mph							9.491	0.75	28.473
Wind Speed = 45 mph							15.689	0.75	47.067
2 	1230	8668.5	15	41	0.5	0.25			
Wind Speed = 5 mph							1.103	2.563	1.614
Wind Speed = 15 mph							9.927	2.563	14.527
Wind Speed = 25 mph							27.574	2.563	40.353
Wind Speed = 35 mph							54.046	2.563	79.091
Wind Speed = 45 mph							89.341	2.563	130.742
3 	738	5992.18	9	41	0.5	0.25			
Wind Speed = 5 mph							0.662	2.563	0.581
Wind Speed = 15 mph							5.956	2.563	5.23
Wind Speed = 25 mph							16.545	2.563	14.527
Wind Speed = 35 mph							32.427	2.563	28.473
Wind Speed = 45 mph							53.604	2.563	47.067
4 	1250	8061.86	12.5	50	0.5	0.25			
Wind Speed = 5 mph							1.121	3.125	1.121
Wind Speed = 15 mph							10.088	3.125	10.088
Wind Speed = 25 mph							28.023	3.125	28.023
Wind Speed = 35 mph							54.924	3.125	54.924
Wind Speed = 45 mph							90.793	3.125	90.793
5 	1200	7315.05	10	60	0.5	0.25			
Wind Speed = 5 mph							1.076	3.75	0.717
Wind Speed = 15 mph							9.685	3.75	6.456
Wind Speed = 25 mph							26.902	3.75	17.934
Wind Speed = 35 mph							52.727	3.75	35.152
Wind Speed = 45 mph							87.162	3.75	58.108
Denotes Changing Variable									

Tail Vane Bending Stress Due To Weight (Y direction)									
Type	Area (in^2)	Izz (lb*in^2)	D1 (in)	C2 (in)	Weight (lb)	b (in)	h (in)	Ix (in^4)	Stress Y (lb/in^2)
	216	4747.77	9	6	0.62	12	0.5	432	0.078
	1230	8668.5	15	20.5	3.55	41	0.5	1.72E+04	0.063
	738	5992.18	9	20.5	2.13	41	0.5	1.72E+04	0.023
	1250	8061.86	12.5	25	3.61	50	0.5	3.13E+04	0.036
	1200	7315.05	10	30	3.47	60	0.5	5.40E+04	0.019
Denotes Changing Variables									

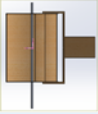




Column1Column2Column3Column4Column5

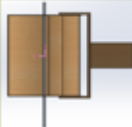




Stresses at the Base of the Tail Vane

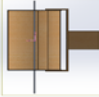



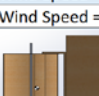
Type	Stress Y (psi)	Stress X (psi)	Total Stresses (psi)	Safety Factor (Yield Strength / combined stress)
 1				
Wind Speed = 5 mph	0.078	0.58	0.55	9154.27
Wind Speed = 15 mph	0.078	5.23	5.19	963.12
Wind Speed = 25 mph	0.078	14.53	14.49	345.11
Wind Speed = 35 mph	0.078	28.47	28.43	175.85
Wind Speed = 45 mph	0.078	47.07	47.03	106.32
 2				
Wind Speed = 5 mph	0.063	1.61	1.58	3157.68
Wind Speed = 15 mph	0.063	14.53	14.50	344.93
Wind Speed = 25 mph	0.063	40.35	40.32	124.00
Wind Speed = 35 mph	0.063	79.09	79.06	63.24
Wind Speed = 45 mph	0.063	130.74	130.71	38.25
 3				
Wind Speed = 5 mph	0.023	0.581	0.57	8774.27
Wind Speed = 15 mph	0.023	5.23	5.22	958.12
Wind Speed = 25 mph	0.023	14.527	14.52	344.46
Wind Speed = 35 mph	0.023	28.473	28.46	175.68
Wind Speed = 45 mph	0.023	47.067	47.06	106.26
 4				
Wind Speed = 5 mph	0.036	1.12	1.103440529	4531.281814
Wind Speed = 15 mph	0.036	10.09	10.07004826	496.52195
Wind Speed = 25 mph	0.036	28.02	28.00501735	178.5394359
Wind Speed = 35 mph	0.036	54.92	54.90600885	91.06471413
Wind Speed = 45 mph	0.036	90.79	90.77500535	55.08124159
 5				
Wind Speed = 5 mph	0.019	0.72	0.71	7065.23
Wind Speed = 15 mph	0.019	6.46	6.45	775.61
Wind Speed = 25 mph	0.019	17.93	17.92	278.95
Wind Speed = 35 mph	0.019	35.15	35.14	142.28
Wind Speed = 45 mph	0.019	58.11	58.10	86.06



## Bending Stress On Support at Enclosure Due to Wind

Type	Area (in <sup>2</sup> )	Izz (lb*in <sup>2</sup> )	D1 (in)	b (in)	h (in)	C1 (in)	Wind Force (Lbf)	Ix (in <sup>4</sup> )	Stress X (Lbf/in <sup>2</sup> )
	281	4747.77	19.75	12	0.5	0.25			
Wind Speed = 5 mph							0.25	0.75	1.66
Wind Speed = 15 mph							2.27	0.75	14.93
Wind Speed = 25 mph							6.30	0.75	41.47
Wind Speed = 35 mph							12.35	0.75	81.28
Wind Speed = 45 mph							20.41	0.75	134.37
	1295	8668.5	25.75	41	0.5	0.25			
Wind Speed = 5 mph							1.16	2.56	2.92
Wind Speed = 15 mph							10.45	2.56	26.26
Wind Speed = 25 mph							29.03	2.56	72.93
Wind Speed = 35 mph							56.90	2.56	142.95
Wind Speed = 45 mph							94.06	2.56	236.30
	803	5992.18	19.75	41	0.5	0.25			
Wind Speed = 5 mph							0.72	2.56	1.39
Wind Speed = 15 mph							6.48	2.56	12.49
Wind Speed = 25 mph							18.00	2.56	34.69
Wind Speed = 35 mph							35.28	2.56	67.99
Wind Speed = 45 mph							58.33	2.56	112.38
	1315	8061.86	23.25	50	0.5	0.25			
Wind Speed = 5 mph							1.18	3.13	2.19
Wind Speed = 15 mph							10.61	3.13	19.74
Wind Speed = 25 mph							29.48	3.13	54.83
Wind Speed = 35 mph							57.78	3.13	107.47
Wind Speed = 45 mph							95.52	3.13	177.66
	1265	7315.05	20.75	60	0.5	0.25			
Wind Speed = 5 mph							1.13	3.75	1.57
Wind Speed = 15 mph							10.21	3.75	14.12
Wind Speed = 25 mph							28.36	3.75	39.23
Wind Speed = 35 mph							55.58	3.75	76.89
Wind Speed = 45 mph							91.88	3.75	127.11

Bending Stress On Support at Enclosure Due to Weight											
	Type	Area (in^2)	Izz (lb*in^2)	D1 (in)	C2 (in)	Weight (lb)	b (in)	h (in)	Iy (in^4)	Stress Y (Lb/In^2)	
1		216	4747.77	19.75	6	0.62	12	0.5	432	0.17	
2		1230	8668.5	25.75	20.5	3.55	41	0.5	1.72E+04	0.109	
3		738	5992.18	19.75	20.5	2.13	41	0.5	1.72E+04	0.05	
4		1250	8061.86	23.25	25	3.61	50	0.5	3.13E+04	0.067	
5		1200	7315.05	20.75	30	3.47	60	0.5	5.40E+04	0.04	
					Denotes Changing Variable						

Stresses on Tail Vane Support at Enclosure (lb)				
Type	Stress Y (Lb/In^2)	Stress X (Lbf/In^2)	Total Stress (psi)	Safety Factor (Yield Strength / Total Stresses)
 1				
Wind Speed = 5 mph	0.17	1.66	1.58	3162.81
Wind Speed = 15 mph	0.17	14.93	14.85	336.80
Wind Speed = 25 mph	0.17	41.47	41.39	120.81
Wind Speed = 35 mph	0.17	81.28	81.20	61.58
Wind Speed = 45 mph	0.17	134.37	134.28	37.23
 2				
Wind Speed = 5 mph	0.11	2.92	2.86	1745.78
Wind Speed = 15 mph	0.11	26.26	26.20	190.83
Wind Speed = 25 mph	0.11	72.93	72.88	68.61
Wind Speed = 35 mph	0.11	142.95	142.89	34.99
Wind Speed = 45 mph	0.11	236.30	236.25	21.16
 3				
Wind Speed = 5 mph	0.05	1.39	1.36	3669.22
Wind Speed = 15 mph	0.05	12.49	12.46	401.22
Wind Speed = 25 mph	0.05	34.69	34.66	144.25
Wind Speed = 35 mph	0.05	67.99	67.96	73.57
Wind Speed = 45 mph	0.05	112.38	112.36	44.50
 4				
Wind Speed = 5 mph	0.07	2.19	2.16	2314.52
Wind Speed = 15 mph	0.07	19.74	19.71	253.72
Wind Speed = 25 mph	0.07	54.83	54.80	91.24
Wind Speed = 35 mph	0.07	107.47	107.44	46.54
Wind Speed = 45 mph	0.07	177.66	177.62	28.15
 5				
Wind Speed = 5 mph	0.04	1.57	1.55	3227.08
Wind Speed = 15 mph	0.04	14.12	14.10	354.53
Wind Speed = 25 mph	0.04	39.23	39.21	127.52
Wind Speed = 35 mph	0.04	76.89	76.87	65.04
Wind Speed = 45 mph	0.04	127.11	127.09	39.34

## Appendix B: Material Detail Matrices

Enclosure/ Blades	Cost (USD)	Strength (psi)	Density (g/m <sup>3</sup> )	Proper size available	Manufacturability (process overview)
Fiberglass	-Epoxy: \$54 (48 oz.) -Fiberglass: \$11.25 (36" x 36") -Surface treating material -Sanding materials -form	Yield: 23099.2 Tensile: 55000 Compressive: 140,000	Glass-fiber: 2.6 Resin: 1.3	Yes	- clean mold - add layer of reinforcement - add epoxy - put in vacuum bag for 24 hrs. - sand - repeat
Rocket body tube	Since appropriate size is not available, no exact value is available.	Tensile: 29595.1	1.3	No	-cut with handsaw *due to the brittleness of the material this process will be slow
Postal Tube	\$70	Slightly less than sonotube	.689	No	- cut with hand saw
Sonotube	\$7/ft (12" dia.) \$23/ft (24" dia.)	Yield: 5000	.689	Yes	- cut with hand saw
Aluminum Sheet Metal	\$25 (36" x 36")	Yield: 13000	2.712	Yes	- cut into size - use sheet metal roller to round
Divinycell	\$28 (36" x 36") *Form must also be purchased	Yield: 1044	.0384	Yes	- heat material and put onto form - will harden as new shape
Owen's Corning Foam *Blades only	\$80 (36" x 36")	Compressive: 15-100	.794	Yes	- Glue layers of foam together - Hot wire cut into shape

Tail Vane	Cost (USD) (36" x 36")	Strength (psi)	Density (g/cm <sup>3</sup> )	Proper size available	Manufacturability (process overview)
Triple Wall Cardboard	\$1.51	Yield: 5000	.689	Yes	- cut with Xacto blade or saw
Balsa Wood	\$25	Flexural: 3140 Compressive: 2160	.198- .433	Yes	- cut with handsaw
Beech Wood	\$157-314	Compressive: 7300 Shear: 2010	1.15- 1.95	Yes	- cut with handsaw
Acrylic	\$82	Yield: 6530	1.2	Yes	- CNC Machining
Aluminum Sheet Metal	\$25	Yield: 13000	2.712	Yes	- CNC Machining
Owen's Corning Foam *Blades only	\$80	Compressive: 15-100	.794	Yes	- Glue layers of foam together - Hot wire cut into shape

